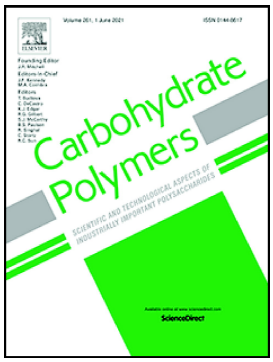

Wood inspired biobased nanocomposite films composed of xylans, lignosulfonates and cellulose nanofibers for active food packaging

José M. Silva, Carla Vilela, Ana Violeta Girão, Pedro C. Branco, João Martins, Mara G. Freire, Armando J.D. Silvestre, Carmen S.R. Freire

PII: S0144-8617(24)00338-2

DOI: https://doi.org/10.1016/j.carbpol.2024.122112

Reference: CARP 122112

To appear in: *Carbohydrate Polymers*

Received date: 2 November 2023

Revised date: 27 March 2024

Accepted date: 29 March 2024

Please cite this article as: J.M. Silva, C. Vilela, A.V. Girão, et al., Wood inspired biobased nanocomposite films composed of xylans, lignosulfonates and cellulose nanofibers for active food packaging, *Carbohydrate Polymers* (2023), https://doi.org/10.1016/j.carbpol.2024.122112

Wood inspired biobased nanocomposite films composed of xylans, lignosulfonates and cellulose nanofibers for active food packaging

José M. Silva[1], Carla Vilela[1], Ana Violeta Girão[2] Pedro C. Branco[3], João Martins[4], Mara G. Freire[1], Armando J. D. Silvestre[1], Carmen S.R. Freire[1]

[1]CICECO – Aveiro Institute of Materials, Department of Chemistry, University of Aveiro, 3810-193, Aveiro, Portugal

[2]CICECO – Aveiro Institute of Materials, Department of Materials and Ceramic Engineering, University of Aveiro, 3810-193, Aveiro, Portugal

[3]RAIZ – Instituto de Investigação da Floresta e Papel, 3800-783 Eixo, Aveiro Portugal

[4]Biotek S.A., 6030-223 Vila Velha de Ródão, Portugal

*Correspondence:

Abstract:

The growing concerns on environmental pollution and sustainability have raised the interest on the development of functional biobased materials for different applications, including food packaging, as an alternative to the fossil fuel-based plastic counterparts, currently available in the market. In this work, functional wood inspired biopolymeric nanocomposite films were prepared by solvent casting of suspensions containing commercial beechwood xylans, cellulose nanofibers (CNF) and lignosulfonates (magnesium or sodium), in a proportion of 2:5:3 wt.%, respectively. All films presented good homogeneity, translucency, and thermal stability up to 153 °C. The incorporation of CNF into the xylan/lignosulfonates matrix provided good mechanical properties to the films (Young's modulus between 1.08 and 3.79 GPa and tensile strength between 12.75 and 14.02 MPa). The presence of lignosulfonates imparted the films with antioxidant capacity (DPPH radical scavenging activity from 71.6 to 82.4%) and UV barrier properties (transmittance ≤ 19.1% (200 – 400 nm)). Moreover, the films

obtained are able to successfully delay the browning of packaged fruit stored over 7 days at 4 ºC. Overall, the obtained results show the potential of using low-cost and eco-friendly resources for the development of sustainable active food packaging materials.

Graphical abstract

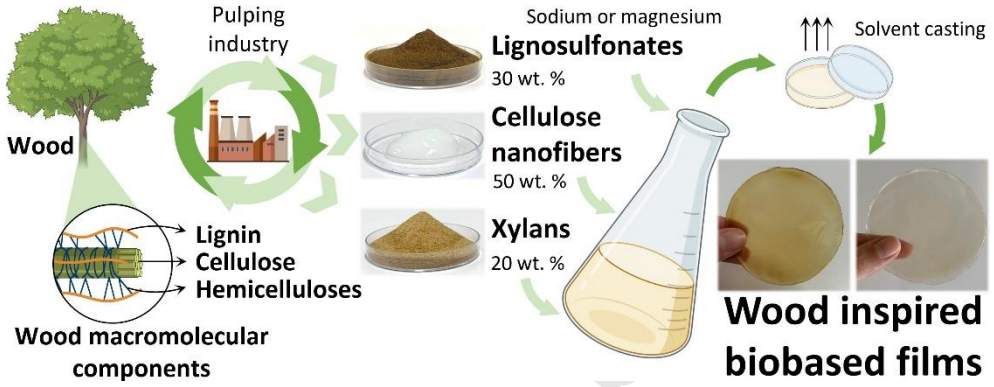

Highlights

- Wood inspired nanocomposite films based on xylan, nanocellulose and lignosulfonates
- Homogeneous and translucent films with good mechanical and thermal performance
- Lignosulfonates endow good UV-barrier and antioxidant properties to the films
- The bioinspired films show potential as eco-friendly materials for active packaging

Keywords: Antioxidant properties; Biobased nanocomposite films; Cellulose nanofibers;
Lignosulfonates; Wood inspired active food packaging; Xylans.

1. Introduction

With the increasing consciousness about environmental pollution risks, the need to reduce the amount of plastic waste has become a pressing issue. Over the last decade, the United Nations (UN) and the European Union (EU) implemented strategies to promote the shift from non-biodegradable petroleum-based products to biodegradable and biobased ones (Fiorentino et al., 2017; United Nations, 2015). Due to this pressure, food packaging industries have been experiencing incredible advances regarding the type of materials used to produce different packaging products. However, nowadays, the challenges on developing new food packaging systems do not address only the replacement of conventional plastics by biobased materials but also search on new ways to improve their shelf-life, and the safety and quality of the packed food, corresponding to the so-called active food packaging (Carvalho et al., 2021; Vilela et al., 2018).

The use of natural polymers, in most cases paired with selected bioactive compounds, is a viable option for the development of eco-friendly active food packaging materials. Several natural polymers and bioactive compounds, like (i) alginate combined with thymol (Karimi-Khorrami et al., 2022), hydrolyzed collagen (Júnior et al., 2021) or sulfur quantum dots (Riahi et al., 2022), (ii) agar blended with essential oils (Mostafavi & Zaeim, 2020), zinc oxide nanoparticles (Roy & Rhim, 2021), beeswax (Zhang et al., 2022) or silver nanoparticles (Roy & Rhim, 2022), (iii) chitosan mixed with essential oils (Flórez et al., 2022), ellagic acid (Vilela et al., 2017) or epigallocatechin-3-gallate loaded melanin-like nanoparticles (Zhao et al., 2022), (iv) keratin combined with pomelo peel pectin (Das et al., 2018) or citric acid (Ramirez et al., 2017), (v) pullulan loaded with titanium oxide nanoparticles (Ghosh et al., 2022; Y. Liu et al., 2019), lysozyme nanofibers (Silva et al., 2018), extracts from chestnut spiny burs and roasted hazelnut skins (Esposito et al., 2020) or carvacrol (Xiao et al., 2022), (vi) starch blended with fruit or tea extracts (Miao et al., 2021) or essential oils

(Chollakup et al., 2020; Vianna et al., 2021) and (vii) xylans combined with CNF and ferulic acid or feruloylated arabinoxylo-oligosaccharides (Moreirinha et al., 2020), lignin extracted from argan nutshells (Halloub et al., 2022) or essential oils (Yousefi et al., 2020), have been investigated as biopolymeric bioactive films for active food packaging purposes.

Wood is a natural composite constituted of cellulose nanofibers embedded in a matrix of hemicelluloses and lignin (Berglund et al., 2020). Cellulose is the major component of wood cell walls, providing strength and rigidity. One of the most common hemicelluloses present in hardwoods, such as eucalyptus, are xylans which are polysaccharides formed of β-1,4-linked xylose residues with side branches of α-arabinofuranose and/or α-glucuronic acids, that contribute to the linkage of cellulose microfibers and lignin in the wood cell walls (Naidu et al., 2018). Lignin is a highly branched aromatic polymer that act as an effective barrier against microbial attacks, and enables water and nutrient transport through plant tissues (Katahira & Elder, 2018). The assembly of these three biopolymers in such an interesting natural material as wood is an inspiration for the design of biobased materials with improved properties. In fact, this combination of biopolymers has already been reported, as a possible way to manufacture functional bioplastics. Specifically, Tedeschi *et al*. (2020), described a process where microcrystalline cellulose, hydrolyzed alkali lignin and xylans from corn core, in different proportions, were dissolved in a mixture of trifluoroacetic acid and trifluoroacetic anhydride, stirred at 80 °C for 45 min and casted into biobased films. However, in this reassembly process, the characteristic features of cellulose are lost in the dissolution step. More recently, Liu *et al*. (2021) prepared biobased films containing microfibrillated cellulose and alkali lignin, by vacuum filtration of suspensions containing the two biopolymers. The produced mats were soaked overnight in a xylan

(from corncob) solution, oven-dried and hot-pressed. The obtained results showed that the cellulose/lignin/xylan mats had superior tensile properties when compared with those without xylans in their composition (L. Liu et al., 2021). Besides being a multi-step process, which is not desirable for scale-up, this methodology has other limitations. Since the cellulose/lignin mats are immersed in an aqueous solution of xylans, it is possible that some lignin of the mats might be redispersed back into the aqueous solution. Furthermore, there is no effective and active way to control the xylans content since their incorporation into the mats occurs via overnight deposition from the aqueous media.

In this context, the present work reports the preparation and characterization of wood inspired biopolymeric nanocomposite films composed of commercial beechwood xylans, cellulose nanofibers and lignosulfonates (magnesium or sodium), by solvent casting for active packaging. Lignosulfonates are lignin derivatives obtained as a side product from the sulfite pulping industry and are normally used as plasticizers in concrete or as a pellet binders in animal feedstocks (Gopinatha Kurup et al., 2019; Theenathayalan et al., 2022). Despite some variability in the chemical composition of wood species, overall, it contains cellulose, between 40 – 50%, hemicelluloses (mainly xylans, in hardwood species, as eucalyptus or beechwood) between 15 – 20% and lignin between 20 – 30% (Neto et al., 2004). Therefore, the relative composition of the developed films was set at 50% of CNF, 30% of lignosulfonates and 20% of xylans, in respect to the total solids content of the films. For comparison purposes, two different types of lignosulfonates were used, namely an industrial sample of magnesium lignosulfonates, since they are an abundant side product a Portuguese pulp and paper industry, and a commercially available sodium lignosulfonate. Finally, glycerol was added to improve the plasticity of the films. The obtained films were characterized

regarding their structure, morphology, thermal stability, optical and mechanical properties, antioxidant activity and moisture uptake capacity to properly assess their suitability for application as biobased active food packaging materials. Lastly, a preliminary evaluation of the performance of the films on the preservation of fresh-cut fruit was carried out.

2. Materials and methods

2.1. Chemicals and materials

Xylan from beechwood (≥ 90%, weight average molecular weight (M_w) ≈ 10.0×10^3 g·mol^{-1}, number average molecular weight (M_n) ≈ 5.29×10^3 g·mol^{-1} and dispersity (Đ) (M_w/M_n) ≈ 1.89, was acquired from Apollo Scientific (Stockport, United Kingdom).

Magnesium lignosulfonates (MgLs) (aqueous solution, < 60 %) obtained from the acidic magnesium-based sulfite pulping of *Eucalyptus globulus* (hardwoods) were supplied by Caima - Indústria de Celulose, S.A. (Constância, Portugal). Lignosulfonic acid sodium salt (NaLs, $M_w \approx 52 \times 10^3$ g·mol^{-1} and $M_n \approx 7 \times 10^3$ g·mol^{-1}, (> 94 %, from softwoods) was acquired from Sigma-Aldrich (St. Louis, Missouri, USA). Cellulose nanofibers (CNF) (2.35 % aqueous suspension) with fibers with an average diameter of 20 – 50 nm and a zeta potential of –12.6 ± 1.5 mV at pH 7 (Silva et al., 2020), was kindly supplied by VTT Technical Research Centre (Espoo, Finland) and obtained from softwood bisulfite fibers by combining mechanical and enzymatic treatments. Glycerol (> 99.5%), 2,2-diphenyl-1-picrylhydrazyl (DPPH) radical and sodium hypochlorite (NaClO) (12.5%) were purchased from Sigma-Aldrich (St. Louis, Missouri, USA). Commercial low-density polyethylene (LDPE) film (thickness 25 ± 5 μm, tensile strength: 5 – 25 MPa, Young's modulus: 0.1 – 0.3 GPa; elongation at break: 100 – 400 %, water vapor transmission rate (WVTR): 2.84×10^{-4} g s^{-1} m^{-2}, water vapor

permeability (WVP): 7.00×10^{-14} g m^{-1} s^{-1} Pa^{-1}, oxygen transmission rate (OTR): 7004 cm^3 m^{-2} day^{-1} and oxygen permeability (OP): 175 cm^3 mm m^{-2} day^{-1} atm^{-1}) (Goodfellow, 2023) was purchased from Sigma-Aldrich (St. Louis, Missouri, USA). Any other chemicals and solvents used were of laboratory grade.

2.2. Preparation of the wood inspired nanocomposite films

The nanocomposite films were prepared by solvent casting of aqueous suspensions containing CNF (50 wt.%, in respect to the total solids content), xylans (20 wt.%), and lignosulfonates (30 wt.%). Initially, the adequate amount of xylan was dispersed in distilled water and left to dissolve under magnetic stirring, at room temperature. After complete dissolution, the adequate amounts of CNF and lignosulfonates were added to the solution and left to stir until full homogenization. Then, glycerol (15 wt.%, in respect to the total solids content), was added and the mixture was stirred for 3 h. Finally, the mixtures were placed into polystyrene petri dishes (94 mm in diameter) and the films were obtained by casting at 40 ºC in a ventilated oven (Thermo Fisher Scientific, Waltham, Massachusetts, USA) overnight. Finally, the films were removed from the molds and stored in a desiccator before characterization. Films without glycerol were prepared following the same procedure for comparison purposes. All films were prepared in triplicate. Table 1 summarizes all nanocomposite films prepared in this study.

Table 1 – Identification, compositions, and thicknesses of the prepared films (different letters above the thickness values correspond to statistically significant differences).

Film	Xylan (mg)	Lignosulfonate (mg)	CNF (mg)	Glycerol (mg)	Thickness (μm)

Be-NaLs-0gly	40	60 (NaLs)	100	-	51 ± 9 [a]
Be-NaLs-15gly	40	60 (NaLs)	100	30	54 ± 4 [a]
Be-MgLs-0gly	40	60 (MgLs)	100	-	48 ± 3 [a]
Be-MgLs-15gly	40	60 (MgLs)	100	30	52 ± 6 [a]

2.3. Characterization techniques

2.3.1. Characterization of the beechwood xylans

The molecular weight values of the xylan sample were determined by size-exclusion chromatography (SEC) using a system equipped with an online degasser, a refractive index detector, and a set of columns comprising a Shodex OHpak SB-G guard column, OHpak SB-802.5HQ and OHpak SB-804HQ columns. The xylan sample in aqueous solution was eluted at a flow rate of 0.5 mL min $^{-1}$ with 0.1 M sodium acetate (aq.) with 0.02 % NaN_3). Before the injection (50 μL), the sample was filtered through a nylon membrane with 0.20 mm pores. The system was calibrated with narrow polyethylene glycol (PEG) standards and the molecular weights were determined by conventional calibration using Clarity software version 2.8.2.648.

The xylan sample was also characterized by ^{1}H and ^{13}C nuclear magnetic resonance (NMR), using a Bruker Avance 300 at 300.13 MHz and 75.47 MHz, respectively using deuterated water as solvent and TMSP as internal reference.

2.3.2. Characterization of the lignosulfonates

The pH of the MgLs and NaLs was determined according to ISO 4316:1977 method. The obtained values of pH were 3.95 ± 0.06 and 9.18 ± 0.06 for MgLs and NaLs, respectively. The MgLs were freeze-dried before use.

2.3.3. Characterization of the films

The attenuated total reflection-Fourier transform infrared (ATR-FTIR) spectra of the films and its individual components were recorded on a PerkinElmer FTIR spectrophotometer (PerkinElmer, Waltham, Massachusetts, USA), equipped with a

single horizontal Golden Gate diamond ATR crystal cell, in the range of 4000 – 500 cm^{-1} by accumulating 32 scans at a resolution of 4 cm^{-1} and intervals of 1 cm^{-1}.

The thickness of the films was measured with a hand-held digital micrometer (MDC-25PX, Mitutoyo Corporation, Tokyo, Japan). The measurements were performed in quintuplicate at randomly selected locations of the films, with an accuracy of 1 μm.

X-ray diffraction (XRD) analysis of the films was performed on a Philips X'pert MPD diffractometer (PANalytical, Almelo, Netherlands) with CuKα radiation (λ = 1.541 Å) at a voltage of 45 kV and a current of 40 mA. The diffractograms were recorded with a scan rate of 0.05° s^{-1} in the range of 5 and 50° in the 2θ scale.

Scanning electron microscopy (SEM) was used to analyze the surface and the cross-section of the obtained nanocomposite films. The micrographs were recorded on a HR-FESEM SU-70 Hitachi microscope (Hitachi High-Technologies Corporation, Tokyo, Japan) at a voltage of 1.0 kV. The energy dispersive X-ray spectroscopy (EDS) was done in the same equipment at a voltage of 15.0 kV equipped with a Bruker QT EDS detector (Billerica, Massachusetts, USA), and the software Esprit 1.9. was used to perform the elemental analysis of the surface of the samples. For the acquisition of the cross-section micrographs, the films were submerged in liquid nitrogen and fractured to properly expose their cross-section areas. Before analysis, all samples were coated with carbon. The surface roughness (the root mean square (RMS)) was determined for an area of 15 × 15 μm^2 using an atomic force microscope (AFM, Bruker Veeco Multimode Nanoscope IIIA (Billerica, Massachusetts, USA)), and the software MountainsLab® v.10.1 was used to accurately represent the typography of the films surface three-dimensionally.

The color parameters of the films were determined using Konica Minolta CM-2300d portable sphere type spectrophotometer (Konica Minolta Sensing Europe B.V.,

Warrington, UK) with horizontal alignment with 2 pulsed xenon lamps and the Spectra Magic^{TM} NX software, after prior calibration with a white calibration plate. The equipment was placed directly on the top of the surface of the samples and the measurements were performed with a d/8 (diffuse illumination, 8-degree viewing angle) system. The color parameters were expressed in the CIELab scale: L^*, lightness: black = 0 and white = 100; a^*, green = $-a^*$ and red = $+a^*$; b^*, blue = $-b^*$ and yellow = $+b^*$ (Moreirinha et al., 2020). The brightness was expressed as the ISO brightness standard (ISO 2470-1). The measurements were performed in triplicate at five randomly selected locations of the films.

Thermogravimetric analysis (TGA) of the films was performed with a Hitachi NEXTA STA300 (Hitachi High-Technologies Corporation, Tokyo, Japan) equipped with a platinum cell. All samples were heated from room temperature up to 800 °C, at a constant rate of 10 °C min^{-1}, under a nitrogen flow of 50 mL min^{-1}.

The ultraviolet-visible (UV-vis) spectra of the films were acquired with a Shimadzu UV1800 UV–vis spectrophotometer (Shimadzu Corporation, Kyoto, Japan), using strips of the films (5×1 cm^2) in the vertical position. The measurements were recorded at room temperature, in the range between 200 and 700 nm, with a step increase of 1 nm.

The tensile mechanical properties of the films were assessed using an Instron 5966 Series equipment (Instron Corporation, Norwood, Massachusetts, USA). The tests were carried out at 24 °C and 43 % relative humidity, using a 500 N static load cell. Initially, the test specimens of the films (5 × 1 cm^2) were placed between two grips with a distance of 3 cm and then stretched with a crosshead velocity of 10 mm·min^{-1}, until breakage. The Young's modulus, tensile strength, and elongation at break were determined with the Instron BlueHill 3 software. At least seven samples of each film were analyzed and used for the determination of the average values of each parameter.

For the determination of the moisture uptake capacity, film samples were cut into squares (1 × 1 cm^2) and stored in a desiccator (20% of relative humidity (RH)) for 72 h, to ensure the same initial moisture content. Afterwards, all samples were weighted and then placed in a closed container and exposed to a 98% RH atmosphere (by exposure of the atmosphere to a saturated aqueous solution of potassium sulfate (K_2SO_4)) at room temperature (O'Brien, 1948). The samples were weighted at different time points during several days, and at least seven samples of each film were analyzed. The moisture uptake values of the films were calculated following (1:

$$\text{Moisture uptake (\%)} = \frac{W_t - W_0}{W_0} \times 100 \quad (1)$$

where W_t and W_0 are the weights of films after t time exposed to the 98% RH atmosphere and the initial weight of the films, respectively (Achachlouei & Zahedi, 2018).

The WVTR and the WVP were determined gravimetrically following the ASTM standard test procedure (ASTM International, 2022) for the water method. Briefly, containers (with a diameter of 3.3 cm) were filled with distilled water (100% RH) up to 2 cm of the top, and were sealed with the prepared films (permeation area of 8.55 cm^2). Then, the film-covered containers were placed in a desiccator with desiccant that had been previously dried at 104 °C for 24 h, to create an atmosphere of 0% RH, at 20 °C. The containers were weighed every hour for 8 h, and five samples of each prepared film were analyzed. All samples were conditioned 24 h prior the test at 23 °C and 50% RH. For comparison purposes, commercial LDPE films were also tested. The WVTR and WVP were calculated using Eq. (2) and Eq. (3), respectively.

$$\text{WVTR (g h}^{-1}\text{ m}^{-2}) = \frac{G}{t \times A} = \frac{G \div t}{A} \quad (2)$$

$$\text{WVP (g m}^{-1}\text{ h}^{-1}\text{ Pa}^{-1}) = \frac{WVTR}{\Delta p} = \frac{WVTR}{S \times (R_1 - R_2)} \times d \quad (3)$$

where G is the steady state weight change (g), t is the time (h), $G \div t$ is the slope obtained by linear regression of humidity weight gain, during a transmission time interval (g h^{-1}), A is the permeation area (m^2), Δp is the vapor pressure difference (Pa), S is the saturation vapor pressure at test temperature (Pa), R_1 is the relative humidity inside the containers (expressed as a fraction), R_2 is the relative humidity inside the desiccator (expressed as a fraction) and d is the thickness of the films (m).

The OP of the films was determined in accordance with the ISO 15105-2:2003, at 23 °C and 50% RH, using a Labthink Perme® OX2/230 equipment (Labthink International, Inc, Medford, Massachusetts, USA), with 5% variability. All samples were conditioned 24 h prior the test at 23 °C and 50% RH. The permeation area was of 5.31 cm^2 and the oxygen concentration in the test gas was 99.96% and the carrier gas was 99.99% nitrogen.

2.4. Antioxidant activity

The antioxidant activity of the films was assessed by the DPPH radical scavenging method following a procedure previously reported (Silva et al., 2018) with light modifications. The films were cut into squares (1 × 1 cm^2) and added to 4 mL of a methanol/water solution (50:50). Afterwards, 250 μL of a DPPH methanolic solution (0.2 mM) was added to the mixtures, and they were kept in the dark at room temperature for 3 h. Later, the mixtures were centrifuged at 6000 rpm for 30 min at room temperature, and the absorbance of the supernatant was measured at 517 nm on a Shimadzu UV1800 UV–Vis spectrophotometer (Shimadzu Corporation, Kyoto, Japan).

The DPPH scavenging activity was calculated using Eq. 4 and all film samples were analyzed in triplicate.

$$\text{DPPH scavenging activity (\%)} = \frac{A_{control} - A_{sample}}{A_{control}} \times 100 \quad (4)$$

where A_{sample} is the recorded absorbance of the samples and $A_{control}$ is the recorded absorbance of the methanol/water solution with 250 μL of the DPPH solution.

2.5. Evaluation of the films' performance on the preservation of a food matrix

Pears (*Pyrus communis* L. cv. Rocha), grown in Portugal, were purchased at a local market in Aveiro (Portugal). Fruits with a diameter between 55 and 60 mm, were chosen according to color uniformity and absence of physical defects. The selected fruits were washed with distilled water, peeled, and cut into halves using a stainless-steel knife. Afterwards, each fruit half was cut into roughly cubed shaped pieces (2.0 × 2.0 × 2.0 cm^3), that were immediately immersed in a NaClO solution at 100 ppm for 10 min for disinfection, followed by immersion in distilled water for 10 min to remove the residues of NaClO. Then, the samples were dried with absorbent paper and placed in aluminum trays coated on the bottom and covered on the top with the prepared films, in sets of 3 pear cubes per tray. After sealing, each container was stored at 4.0 ± 1.0 °C for 7 days. For comparison purposes, samples with no film, and with commercial LDPE films were prepared. To assess the performance of the produced films as active packaging systems, the pear samples were analyzed on the 3rd and 7th day of storage regarding their visual appearance, browning index (BI), weight loss and pH.

The visual appearance of the fruit samples was recorded using the Konica Minolta CM-2300d portable sphere type spectrophotometer (Konica Minolta Sensing Europe B.V., Warrington, UK) with horizontal alignment with 2 pulsed xenon lamps. The

equipment was placed directly on the top of the surface of the samples and the measurements were performed with a d/8 (diffuse illumination, 8-degree viewing angle) system and the Spectra Magic^{TM} NX software was used to determine the color parameters. The color measurements were obtained at five random sites of the fruit cubes surfaces and performed in triplicate for each aluminum tray. The obtained parameters were also expressed in the CIELab scale and were used to calculate the fruit BI, according to Eq. (5) (Palou et al., 1999).

$$\text{Browning index (BI)} = \frac{[100(X-0.31)]}{0.172} \quad (5)$$

where $X = \frac{(a^*+1.75L^*)}{(5.64L^*+a^*-3.012b^*)}$.

The weight loss of the fruits was determined from the difference between the initial weight of each fruit cube (W_i) and its respective weight at day n of the storage (W_n), using Eq. (6) (Longwei et al., 2021). These measurements were performed in triplicate.

$$\text{Weight loss (\%)} = \frac{W_i - W_n}{W_i} \times 100 \quad (6)$$

The pH of the fruit samples was assessed according to the AOAC 981.12 method. Briefly, 10 g of fruit were grinded with a hand blender with 100 mL of distilled water, before measuring the pH of the solution using a digital benchtop pH meter (pH 50 VioLab benchtop pHmeter, XS Instruments, Carpi, Italy). Five measurements were carried out for each sample (Rodríguez et al., 2020).

2.6. Statistical analysis

The statistical analysis was performed with GraphPad Prism 9 (GraphPad Software Inc., San Diego, California, USA). All data was treated with at least three replicates, and

the results are presented as mean ± standard deviations. The obtained results were statistically analyzed with a confidence level of 95%, with the ANOVA test to compare the significant differences between them. A value of $p < 0.05$ was considered statistically significant and Tukey's multiple comparison test was used for a pairwise comparison of the means.

3. Results and discussion

Wood inspired biobased nanocomposite films were prepared by solvent casting of aqueous suspensions containing wood xylans, CNF, and lignosulfonates in a mass proportion of 20:50:30. Fig. 1 presents a schematic illustration of the preparation procedure of the wood inspired nanocomposite films.

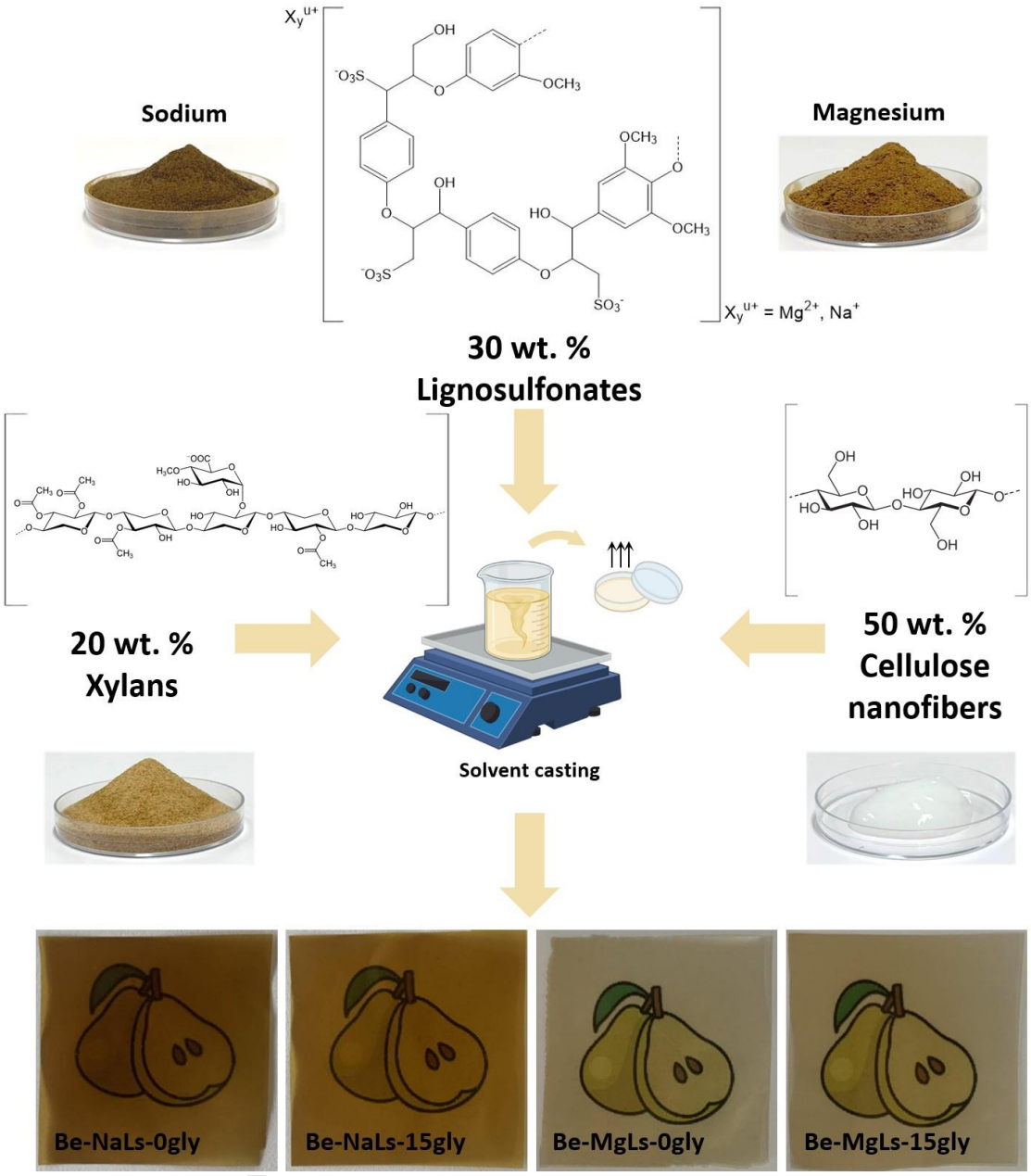

Fig. 1 - Schematic illustration of the preparation procedure and digital photographs of the wood inspired nanocomposite films. The films are placed on top of a drawing of a pear to evidence their translucency.

Based on the role of cellulose, lignin and hemicelluloses in wood, it is expected that xylans and lignosulfonates act as polymeric matrices of the nanocomposite. Additionally, lignosulfonates were added as functional additives to impart the films with antioxidant and UV-barrier properties, and to contribute to the overall cohesivity of

the films (Núñez-Flores et al., 2012). CNF was incorporated as the reinforcing component, i.e. to enhance the tensile strength and toughness of the biobased films, as cellulose fibers do in the wood cell walls. Finally, glycerol was added as plasticizer, to improve the handling, toughness, and flexibility of the films.

All the obtained nanocomposite films were then characterized in terms of their structure, morphology, optical properties, mechanical performance, thermal stability, antioxidant activity and moisture uptake capacity to evaluate their potential for application as active food packaging materials. To corroborate the obtained results, a preliminary study on the ability of the films to preserve fresh-cut fruit was also performed.

All the prepared films were very homogeneous, translucent and their colors varied from an ochre yellow to a pale yellow, as shown in Fig. 1. The color of these biobased films is essentially associated with the intrinsic color of the lignosulfonates, with the NaLs originating darker films than the MgLs counterparts. Membranes containing NaLs in combination with bacterial nanocellulose have been reported to have similar colors (Vilela et al., 2020). The thickness of the produced films ranged from 48 ± 3 to 54 ± 4 μm (Table 1), with no significant differences between them, which is in line with their similar compositions (relative proportions of the different components) and high homogeneity.

3.1. Structural and morphological characterization

The chemical structure of the produced films, and of their individual components for comparison purposes, was studied by ATR-FTIR spectroscopy (Fig. 2 (A)). The spectrum of the xylan used in this study presents the typical vibrations of polysaccharides (Morais et al., 2018; Sun et al., 1998), with the main vibrations at 890

cm^{-1} (C–O stretching of the glycosidic bond, between the xylopiranose units of the main xylan chain structure), 1034 cm^{-1} (C–O–C stretching of the pyranoid-rings), 1143 cm^{-1} (C–OH elongation), 1450 cm^{-1} (C–H bending), 1605 cm^{-1} (C–C stretching) and 3354 cm^{-1} (O–H stretching vibrations) (Sousa et al., 2016).

The spectra of both lignosulfonates (NaLs and MgLs) used in this study are in accordance with data reported in the literature, with the main vibrations at 620 cm^{-1} (C–S stretching), 1040 cm^{-1} (C–H and C–O–C stretching), 1170 cm^{-1} (S=O stretching), 1417 cm^{-1} (C–O stretching and C–H bending), 1604 cm^{-1} (C–C stretching) and 3334 cm^{-1} (O–H stretching) (Q. Shen et al., 2008; Vilela et al., 2020). The ATR-FTIR spectrum of CNF presented a typical profile of a cellulosic substrate with absorption peaks at 1031 cm^{-1} (C–O–C stretching of the cellulose backbone polymer), 1161 cm^{-1} (C–O–C asymmetric stretching), 1335 cm^{-1} (O–H bending), 2900 cm^{-1} (C–H stretching) and 3300 cm^{-1} (O–H stretching) (Foster et al., 2018). The spectrum of glycerol shows the typical absorption peaks at 890 cm^{-1} (C–O stretching), 1040 cm^{-1} (C–O–H stretching of the bonds of C1 and C3 carbons), 1143 cm^{-1} (C–O-H stretching of the bond of C2 carbon), 2920 cm^{-1} (C–H stretching) and 3300 cm^{-1} (O–H stretching) (Basiak et al., 2018). The ATR-FTIR spectra of all nanocomposite films are very similar, as expected considering their comparable compositions. The films display the main vibrations peaks of the different components, as described above, and no deviations are observed.

The chemical structure of the xylan was also characterized by NMR, and the obtained ^{1}H NMR spectrum presented the typical xylan proton resonances, namely at 4.38, 4.00, 3.68, 3.45 and 3.19 ppm. The peak at 3.24 ppm corresponds to the 4-OCH_3 of 4-O-Methylglucuronic acid moieties (Li et al., 2016; Morais et al., 2018; Pastell et al., 2009). In the ^{13}C NMR spectrum, five main resonances were observed at δ 102.2, 73.2, 74.4, 77.0 and 63.5 ppm, assigned to the carbons of the β-D-xylopyranose units.

The peak at 59.9 ppm relates to the 4-OCH_3 resonance, being in accordance with the ^1H spectrum previously described (Li et al., 2016; F. Peng et al., 2009; P. Peng et al., 2011).

The obtained films were also characterized by XRD analysis (Fig. 2 (B)). All films presented the XRD pattern of cellulose I, with the well-known peaks at 2θ = 14.5º, 16.8º and 22.9º, which correspond to the (101), ($10\bar{1}$) and (002) diffraction planes, respectively (Foster et al., 2018; Gong et al., 2017). The addition of glycerol to the nanocomposite films increased their amorphous character as reported in the literature (Gonçalves et al., 2019).

The morphology of the films was assessed by SEM, and their surface and cross-section micrographs are displayed in Fig. 3 (A) and (B). All films present homogeneous and uniform surfaces, with cross-sections evidencing a good distribution of the different components without the formation of agglomerates of cellulose nanofibers. This trend proves the good compatibility of all components in the preparation of biofilms. In fact, these results were expectable given the film-forming capacity of most of these biopolymers and their intrinsic compatibility, as in wood and plants. These observations are also in agreement with the visual aspect of the films discussed above (Fig. 1). The surface micrographs of both films show some aggregates, more evident in those with NaLs. The EDS analysis performed on different places at the surface of films (with and without aggregates) are displayed in Fig. 3 (C) and (D), showing that these aggregates are indeed mainly composed of lignosulfonates because of the higher intensity of sodium or magnesium peaks in these regions. The differences between the films with the two lignosulfonates are certainly related with the wood species used as raw material (softwood vs. hardwood) and the manufacturing process (neutral sulfite semi-chemical

pulping vs. sulfite process) used to produce the lignosulfonates, that may impart them with different characteristics (Aro & Fatehi, 2017; Leon-Tinoco et al., 2022).

The roughness of the surface of all prepared films was also evaluated by AFM and the 3D model typography of the films surfaces are presented in Fig. 4. The results show a clear tendency of the films roughness decreasing with the addition of glycerol (Be-NaLs-0gly: 116.6 ± 6.9 nm; Be-NaLs-15gly: 74.9 ± 8.6 nm) (Be-MgLs-0gly:115.8 ± 16.5 nm; Be-MgLs-15gly: 72.9 ± 7.4 nm). Furthermore, there are no significant differences in the films roughness regarding the different type of lignosulfonate, showing that the distinct aggregates observed on the micrographs of the film surfaces do not result in different roughness values.

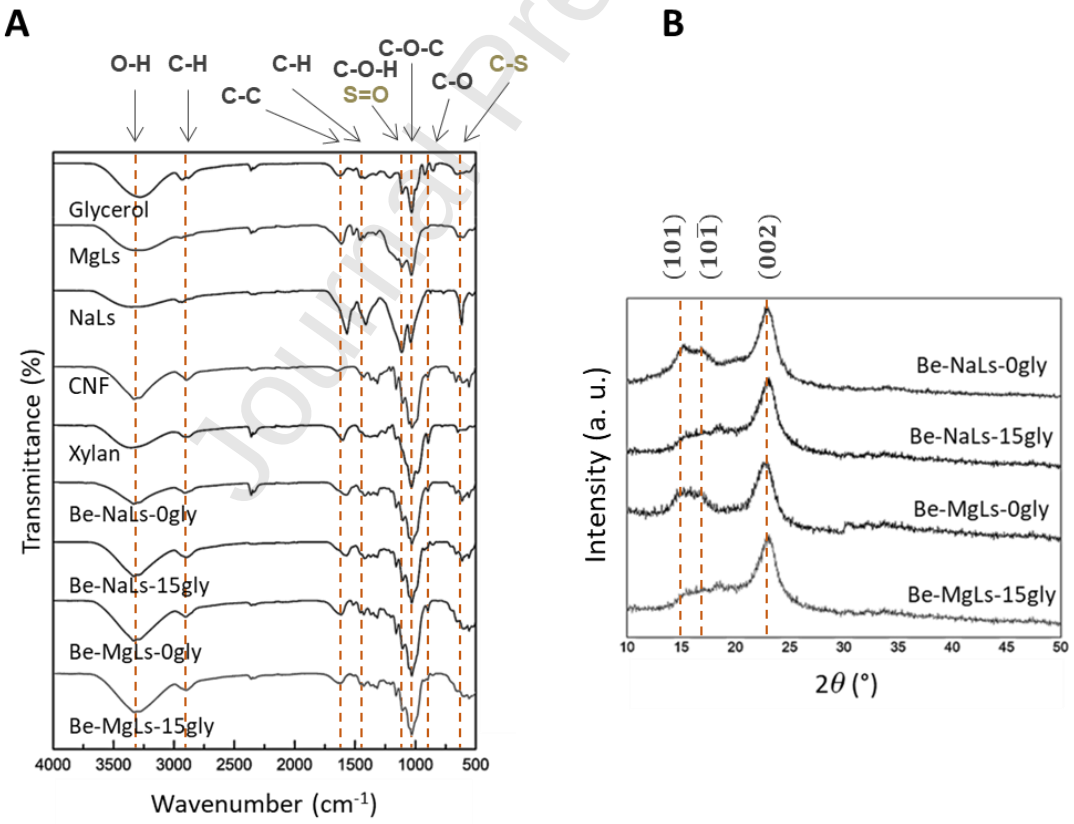

Fig. 2 - (**A**) ATR-FTIR spectra of the films and their individual components and (**B**) XRD patterns of the prepared films.

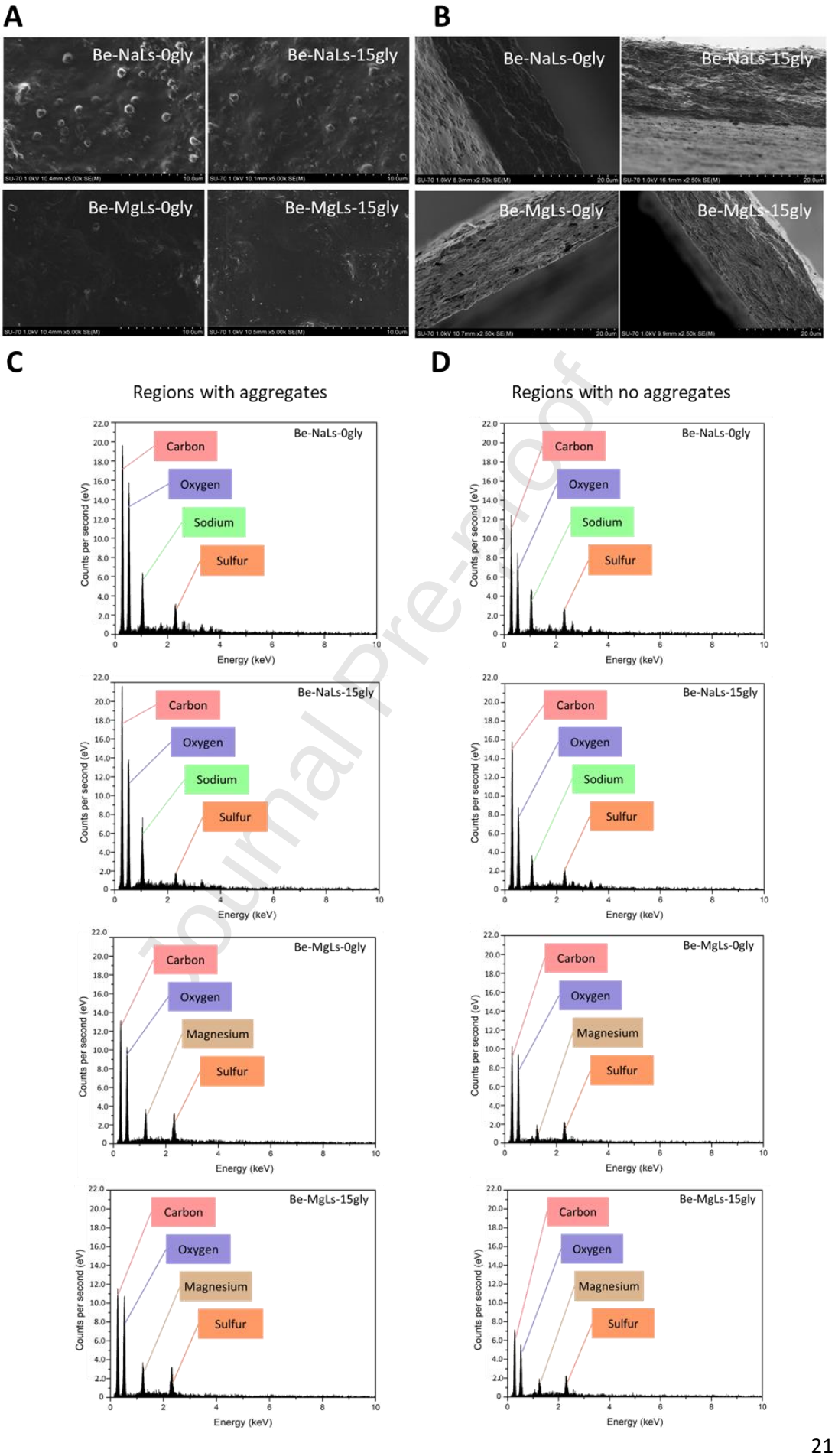

Fig. 3 - (**A,B**) SEM micrographs of surface (**A**) and cross-section (**B**) of the films and EDS spectra of the films surfaces in the regions with aggregates (**C**) and in the regions without aggregates (**D**).

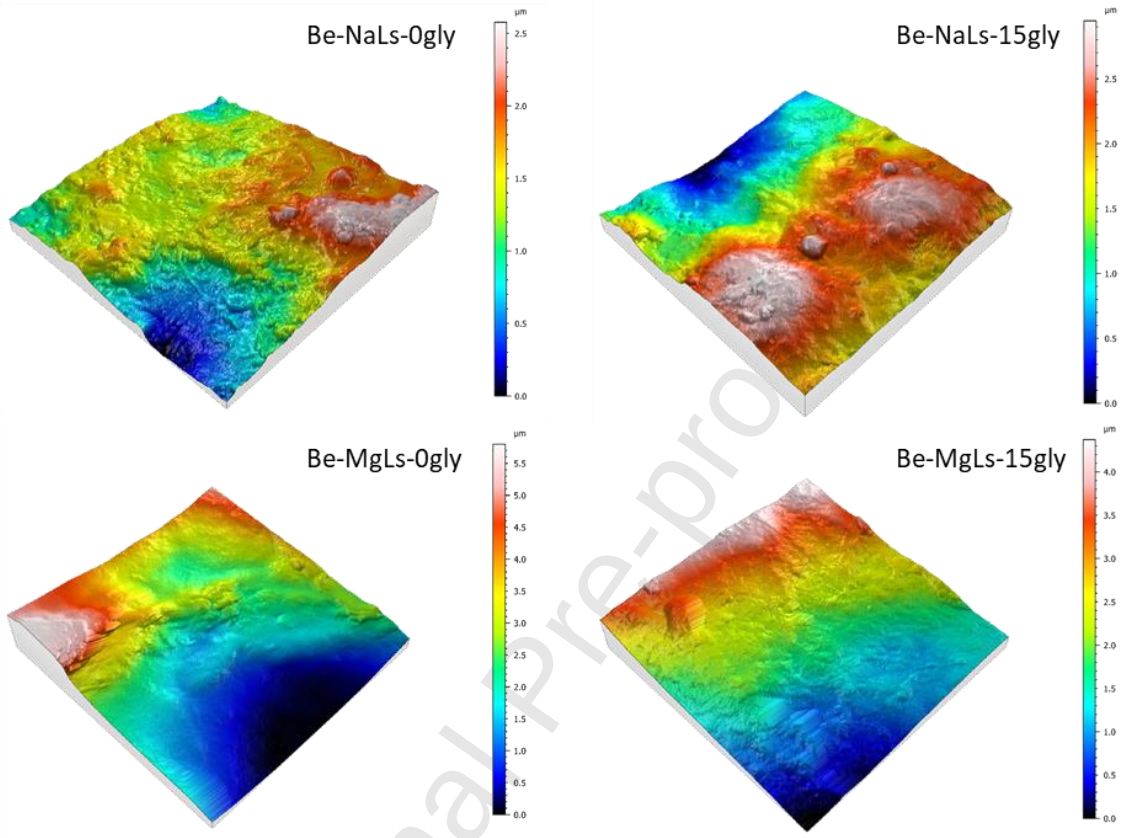

Fig. 4 – 3D representation of the typography of the produced films obtained from AFM analysis.

3.2. Thermal stability, mechanical properties and moisture uptake capacity

The thermal stability and degradation profiles of the nanocomposite films, and their individual components, were assessed by thermogravimetric analysis under nitrogen atmosphere. The obtained thermograms are displayed in Fig. 5 (A).

The thermal degradation profile of xylan exhibits a double-step weight loss, in the temperature range of 150 – 600 °C, with a weight loss occurring at 243 °C, associated with the cleavage of side-chain structures, such as 4-*O*-methylglucuronic acid moieties. The additional weight loss occurs at 292 °C, which is ascribed to the degradation of the

main hemicellulose polymer chain (Fu et al., 2019; Shafizadeh et al., 1972; D. K. Shen et al., 2010).

The thermogram of CNF exhibits a single-step degradation profile, with a maximum degradation temperature of 336 °C, assigned to the cleavage of the β-(1-4) glycosidic bonds of the cellulosic polymer chain (Yang et al., 2007).

Both lignosulfonates underwent double-step degradation processes. While the MgLs display maximum decomposition temperatures of 300 and 608 °C, the NaLs present maximum decomposition temperatures of 250 and 687 °C. The first step of the lignosulfonates decomposition accounts for the release of water, and low molecular weight organic molecules resulting from the degradation of the organic part of the lignosulfonates. The second decomposition step corresponds to the loss of CO_2 produced on the decomposition of magnesium carbonate ($MgCO_3$) and sodium carbonate (Na_2CO_3), formed during the previous thermal degradation of MgLs and NaLs (Jakab et al., 1991; Lemes et al., 2010).

The lack of clear and sharp peaks during the thermal degradation of the lignosulfonates is due to the structural complexity and the heterogeneity of their lignin derived structure, from which their thermal decomposition occurs by several competing reactions in the course of which its various bonds are cleaved at different temperatures depending on the bond energies (Lemes et al., 2010; Myrvold, 2008). At the end of the analysis (800 °C), NaLs and MgLs left a residue of *ca*. 41.6 and 34.8%, of the initial mass, respectively.

Regarding the nanocomposite films, they all presented three distinct mass loss stages. The first stage is in the temperature range of 30 – 153 °C, and is related to the volatilization of the adsorbed water molecules from the films. The second one is in the temperature range of 150 – 500 °C. In this stage, the MgLs films present degradation

peaks at 257 and 343 °C (Be-MgLs-0gly) and at 299 and 346 °C (Be-MgLs-15gly), which are attributed to the degradation of CNF and xylans present in the film. The degradation of the MgLs fraction also occurred in this temperature stage. These peaks present a small increase in the temperatures of maximum degradation, when compared to their individual components, revealing that the good compatibility of all films components improved the thermal stability of the nanocomposites. These results concur with other works already reported in the literature, where the incorporation of CNF into xylans based films enhanced their thermal stability (Moreirinha et al., 2020). Similarly, in this temperature range, the NaLs films present degradation peaks at 235 and 297 °C (Be-NaLs-0gly) and at 207 and 304 °C (Be-NaLs-15gly). The lower maximum degradation temperatures of these films, when compared to the ones containing the MgLs, are attributed to the thermal stability profile of the NaLs, that showed lower maximum thermal degradation temperatures in this range (250 °C) than the MgLs (300 °C), as mentioned before. As expected, the films plasticized with glycerol degrade at lower temperatures (Be-MgLs-15gly: 163 °C; Be-NaLs-15gly: 152 °C) when compared to films without glycerol (Be-MgLs-0gly: 208 °C; Be-NaLs-0gly: 198 °C) due the decomposition of glycerol that occurs between 125 – 240 °C (López et al., 2015; Mena-Cervantes et al., 2020). The third mass loss stage of the films occurs in the temperature range of 502 – 800 °C. In this stage, both MgLs films present a very small, near imperceptible degradation peak at 609 (Be-MgLs-0gly) and 613 °C (Be-MgLs-15gly) attributed to the decomposition of $MgCO_3$. The NaLs films present a more noticeable degradation peak at 713 (Be-NaLs-0gly) and 716 °C (Be-NaLs-15gly) that correspond to the decomposition of Na_2CO_3 (Lemes et al., 2010).

At the end of the analysis, the final residue left of the films were 30.8% (Be-MgLs-0gly), 22.2% (Be-MgLs-15gly), 38.5% (Be-NaLs-0gly) and 27.6% (Be-NaLs-15gly) of the initial masses.

In conclusion, all films exhibit thermal stability up to 153 °C, which is a key feature considering their applicability as food packaging materials. This high temperature allows them to withstand typical sterilization procedures required for food-based applications that normally take place around 121 – 135 °C (Ansari & Datta, 2003).

The mechanical properties of the films were determined by tensile experiments, and the most relevant parameters, namely the Young's modulus, the elongation at break and the tensile strength, obtained from the stress-strain curves are presented in Fig. 5.

Regarding the two lignosulfonates, the obtained results show that there are no significant differences between the tensile strength of the different films. Similarly, for the non-plasticized films, the Young's modulus presents similar values, regardless of the type of lignosulfonate. However, the plasticized films with MgLs display a Young's modulus value lower than the films with NaLs, resulting in higher values of elongation at break. When comparing the films with different content of plasticizer, it is clear that the addition of glycerol turns the films less stiff, as demonstrated by the decrease of the Young's modulus and concomitant increase of the elongations at break. Similar trends have been observed for other polysaccharides-based films, such as alginate, where the increase of glycerol from 10 to 30% led to a decrease in the Young's modulus of the films from 934 to 15 MPa and to an increase in the elongation at break from 12 to 21% (Gao et al., 2017), or xylan based films, where the increase of glycerol from 0 to 25 % led to an decrease in the Young's modulus of the films from 3173.4 to 917.2 MPa and to an increase in the elongation at break from 1.9 to 2.6% (Sousa et al., 2016). This behavior is due the incorporation of the plasticizer molecules into the polymer matrix.

Due the abundance of hydroxy groups, the plasticizer can establish intermolecular hydrogen bonds with other components of the material, namely the lignosulfonates, cellulose nanofibers and xylan, weakening the attractive forces between more adjacent macromolecules, therefore, increasing the spacing between the polymer chains in the material, reducing intermolecular interactions, which allows for greater mobility and flexibility of the material (Eslami et al., 2023).

When compared with commonly available plastic films used for food packaging, the prepared biobased ones, present mechanical properties similar to poly(ethylene-vinyl acetate) (EVA) (tensile strength of 6 – 19 MPa) and LDPE (tensile strength of 7 – 25 MPa) films of similar thicknesses (± 50 µm), and higher elongations at break than polystyrene films (2 – 3%) (Bastarrachea et al., 2011; Schnell et al., 2017). These values are also similar to the tensile strength of thinner LDPE films (25 ± 5 µm; tensile strength of 5 – 25 MPa), as stated by the manufacturer (Goodfellow, 2023). Therefore, the developed wood inspired films should endure the mechanical stress associated with handling, storage, and transportation of food packaging systems.

The hydrophilic nature of xylans, CNF and lignosulfonates makes the nanocomposites films moisture sensitive, and therefore, it is important to evaluate their interaction with water. The water sorption isotherms of the produced films are presented in Fig. 5 (C). The results show that all films have very similar moisture uptake profiles, however, the films without glycerol display significantly lower moisture uptake values (Be-NaLs-0gly: 171.5 ± 8.0%; Be-MgLs-0gly: 174.2 ± 6.5%), when compared to those with glycerol (Be-NaLs-15gly: 265.4 ± 6.0%; Be-MgLs-15gly: 261.9 ± 2.8%). This increase in the moisture uptake capacity of the plasticized films is a well-known trend (Basiak et al., 2018; López et al., 2015), and it was expected, due the hydrophilic and

hygroscopic nature of glycerol, allied with the increased space between the polymer chains of the material that the incorporation of plasticizer promotes.

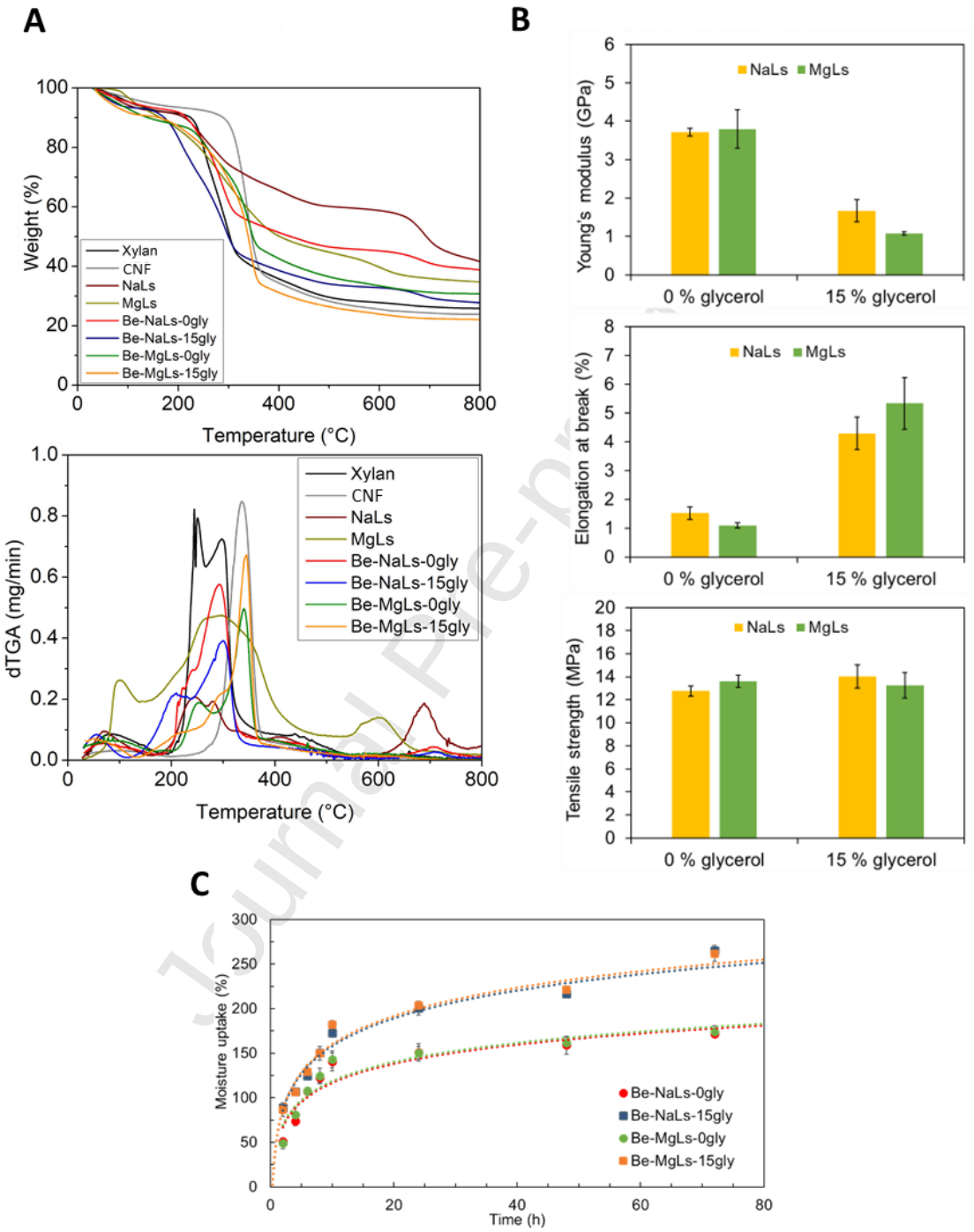

Fig. 5 – (**A**) TGA tracings (on the top) and corresponding derivatives (on the bottom), (**B**) Young's modulus, elongation at break, and tensile strength and (**C**) moisture uptake capacity of the produced films.

3.3. Water vapor and oxygen barrier properties

The water and oxygen barrier properties have a major impact on maintaining or extending the shelf-life of packaged foods, since the efficacy of packaging is normally related to its barrier capacity. Thus, water vapor transmission rate and water vapor permeability of the prepared films and of the LDPE films were studied. The results are presented in Table 2. The commercial LDPE films presented the lowest WVTR and WVP values ($4.40 \pm 0.24 \times 10^{-4}$ g s^{-1} m^{-2} and $6.84 \pm 0.37 \times 10^{-14}$ g m^{-1} s^{-1} Pa^{-1}, respectively), as expected. These values are in accordance with the WVTR ($1.74 – 36.9 \times 10^{-4}$ g s^{-1} m^{-2}) and WVP ($6.67 – 8.70 \times 10^{-14}$ g m^{-1} s^{-1} Pa^{-1}) data described in the literature for LDPE films with similar thicknesses (Bastarrachea et al., 2011; Battisti et al., 2017; Kibar & Us, 2017) and with the data provided by the manufacturer (WVP = 7.00×10^{-14} g m^{-1} s^{-1} Pa^{-1} and WVTR = 2.84×10^{-4} g s^{-1} m^{-2} (Goodfellow, 2023)). The prepared biobased films presented higher water vapor transmission values than those attained for LDPE films. These results are also in agreement with previous reports found in the literature (Tedeschi et al., 2020), where films composed of microcrystalline cellulose, hydrolyzed alkali lignin and xylans present higher WVTR and WVP values (ranging between $8.51 – 11.0 \times 10^{-2}$ g s^{-1} m^{-2}, to the WVTR and between $1.25 – 1.97 \times 10^{-9}$ g m^{-1} s^{-1} Pa^{-1} to the WVP). Moreover, the obtained results show that there are no significant differences between the values of the films with the two different lignosulfonates, suggesting that their different nature do not affect the water vapor barrier properties of the films. However, when comparing the films with and without glycerol, it is possible to observe that the films containing plasticizer present the highest WVTR and WVP values. This was expected since the incorporation of glycerol increases the space between the polymer chains of the material, allowing a higher volume for water

vapor to pass through per area of film per time. This tendency is well documented in the literature (Andrade-Pizarro et al., 2015; Cerqueira et al., 2012; Eslami et al., 2023).

The oxygen permeability rate is considered one of the most relevant properties in the development of a packaging material. Oxygen is responsible for causing oxidation of certain components in food, such as fats, oils or vitamins (Yildirim et al., 2018). Therefore, to ensure the maximum shelf-life and safety of packaged foods, it is essential that a packaging material has a low oxygen permeability rate. Thus, in this work a preliminary evaluation of the oxygen permeability coefficient and oxygen transmission rate of the prepared films was carried out. The results show that the films prepared with MgLs present OTR and OP values of one order of magnitude inferior to their NaLs counterparts (OTR = Be-NaLs-15gly: 2940 cm^3 m^{-2} day^{-1} and Be-MgLs-15gly: 158 cm^3 m^{-2} day^{-1}; OP = Be-NaLs-15gly: 153 cm^3 mm m^{-2} day^{-1} atm^{-1} and Be-MgLs-15gly: 5 cm^3 mm m^{-2} day^{-1} atm^{-1}). All values are lower than those reported in the literature for LDPE films of similar thicknesses (6314 cm^3 m^{-2} day^{-1}) (Bhatia et al., 2013) and lower than the values reported by the manufacturer, for the used LDPE film (OTR: 7004 cm^3 m^{-2} day^{-1}; OP: 175 cm^3 mm m^{-2} day^{-1} atm^{-1} (Goodfellow, 2023)), indicating that the prepared films are a viable and functional solution for packaging of oxygen sensitive foods.

Table 2 – WVTR, WVP and OP of the prepared films and LDPE films, for comparison purposes (different letters above the values correspond to statistically significant differences). n.d. – non determined value.

Film	WVTR ($\times 10^{-4}$ g s^{-1} m^{-2})	WVP ($\times 10^{-14}$ g m^{-1} s^{-1} Pa^{-1})	OTR (cm^3 m^{-2} day^{-1})	OP (cm^3 mm m^{-2} day^{-1} atm^{-1})
LDPE	4.40 ± 0.24 [a]	6.84 ± 0.37	n.d.	n.d.

		[a]		
Be-NaLs-0gly	16.76 ± 0.34 [b]	58.19 ± 1.18 [b]	n.d.	n.d.
Be-NaLs-15gly	20.64 ± 0.74 [c]	81.50 ± 2.91 [c]	2940	153
Be-MgLs-0gly	16.54 ± 0.46 [b]	58.14 ±1.62 [b]	n.d.	n.d.
Be-MgLs-15gly	20.48 ± 0.41 [c]	79.71 ± 1.58 [c]	158	5

3.4. Optical properties

The optical properties of the films were first assessed by measuring the CIELab parameters (*L**, lightness: black = 0 and white = 100; *a**, green = – *a** and red = + *a**; *b**, blue = – b* and yellow = + *b**) and the ISO brightness standard (ISO 2470-1).

As displayed in Fig. 6 (B), the films containing NaLs show a significantly lower lightness (*L**) (Be-NaLs-0gly: 35.98 ± 2.43; Be-NaLs-15gly: 34.50 ± 2.65) when compared with the ones containing MgLs (Be-MgLs-0gly: 78.26 ± 1.66; Be-MgLs-15gly: 78.89 ± 1.16). The same tendency is observed for the ISO brightness parameter (Be-NaLs-0gly: 4.96 ± 0.66; Be-NaLs-15gly: 4.69 ± 1.13; Be-MgLs-0gly: 39.63 ± 2.19; Be-MgLs-15gly: 41.56 ± 1.37). These values are in accordance with the visual aspect of the films (Fig. 1), since the ones containing NaLs are considerably darker. Even though the yellowness of the films does not vary to a great extent with values of *b** similar for all obtained film, the redness of the films is slightly different, with films with NaLs showing higher *a** values. Similarly to the *L**, the color parameters *a** (greenness/redness) and *b** (blueness/yellowness) also corroborate the films visual appearance (Fig. 6 (A)). These differences confirm that the color of the films is related mainly with the intrinsic color of the lignosulfonates.

The optical barrier properties of the produced films were studied by UV–Vis spectroscopy in the wavelength range of 200 and 700 nm. The obtained spectra are

presented in Fig. 6 (C) and reveal transmittance values between 0 and 19.1 % in the ultraviolet range (200 – 400 nm) and 0.7 – 41.0 % in the visible range (400 – 700 nm). Overall, all films exhibit UV-absorbing properties in the upper range of UVC (200 – 280 nm, short-wavelength radiation), UVB (280 – 320 nm, short-wavelength radiation) and UVA (320 – 400 nm, long-wavelength radiation) regions. This behavior is in agreement with previous reported results for other films containing alkali lignin and cellulose nanocrystals, where all UV radiation from 200 - 320 nm was absorbed (Halloub et al., 2022). In agreement with the color parameters, the films containing NaLs, which present lower lightness values, also display significantly lower transmittance values in the UVA (ranging from 0 – 0.9 %) and visible regions (ranging from 0.7 – 40.2%), when compared to their MgLs counterparts (0.1 – 19.1% and 18.7 – 41.0%, respectively). Overall, all films present good UV blocking properties, blocking nearly all the UV radiation. Therefore, these films can be applied as active packaging systems, helping in preventing the degradation of light-sensitive foods, and thus expanding the shelf-life of these packed products (Vilela et al., 2018; Yildirim et al., 2018).

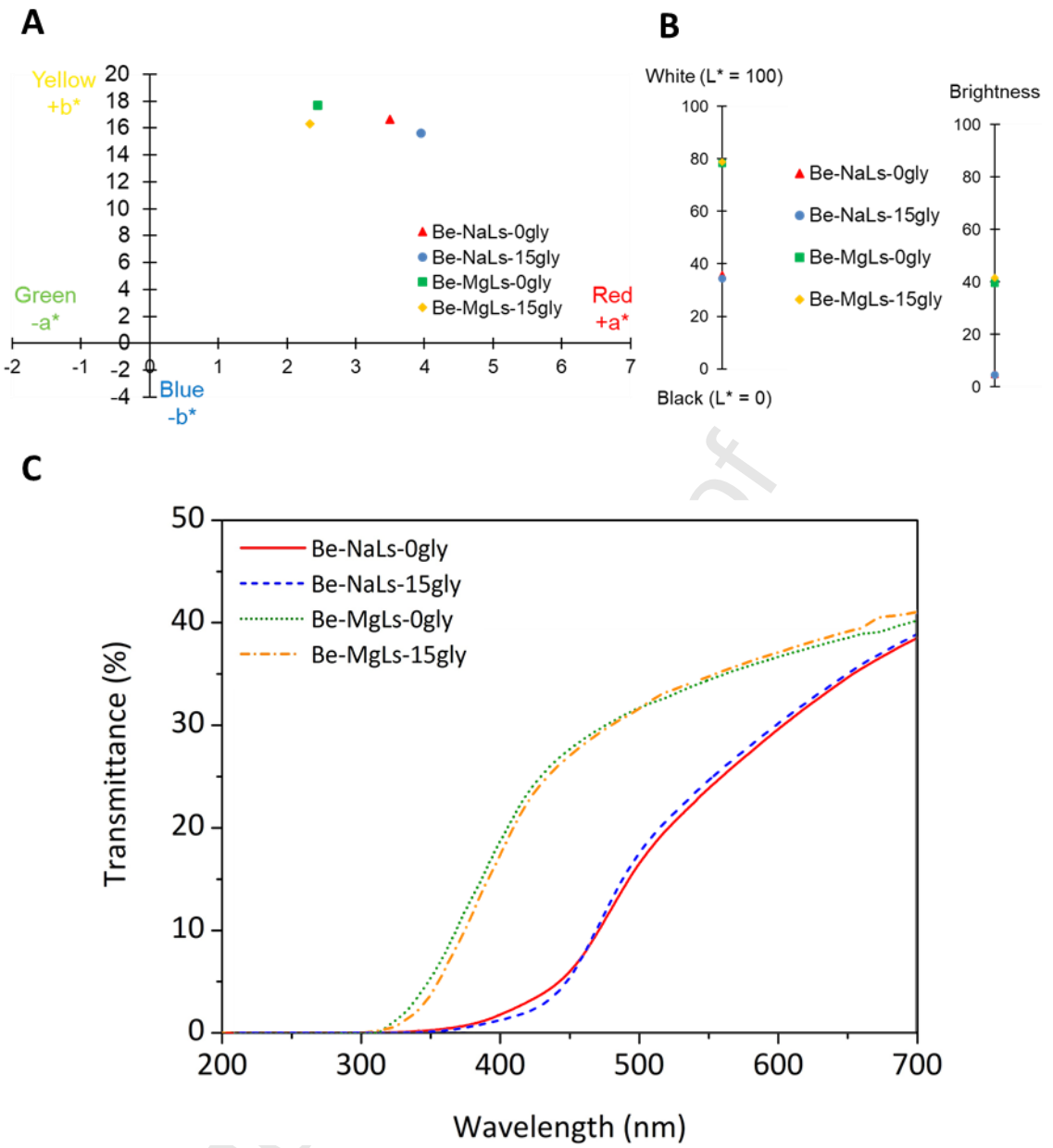

Fig. 6 - Color parameters (**A**) *a** and *b** and (**B**) *L** and brightness and UV-vis spectra of the nanocomposite films (**C**).

3.5. Antioxidant activity

Antioxidants are known for reducing oxidative degradation, and their integration into biobased nanocomposite films plays an important role on imparting them with active functions that will help extending the foods shelf life and maintaining their

quality and freshness (Silva et al., 2018; Vilela et al., 2018). The antioxidant activity of the produced films was assessed by the DPPH radical scavenging assay, and the results are presented in Fig. 7.

The incorporation of lignosulfonates into the films conveyed a very high radical scavenging activity (Fig. 7), with DPHH values of 71.5 – 71.8 % for the NaLs films, and 80.3 – 82.4 % for the MgLs ones. The good antioxidant properties of the lignosulfonates, is related to their complex structure with abundant phenolic moieties capable of acting as free-radical scavengers (Alexandri et al., 2016; Núñez-Flores et al., 2012). The films studied here display higher antioxidant capacities than other materials with similar contents of cellulose and alkali lignin (20 wt.% lignin, scavenging activity = 42.6% (L. Liu et al., 2021). It was also observed that the addition of glycerol did not significantly impact the antioxidant capacity of the films.

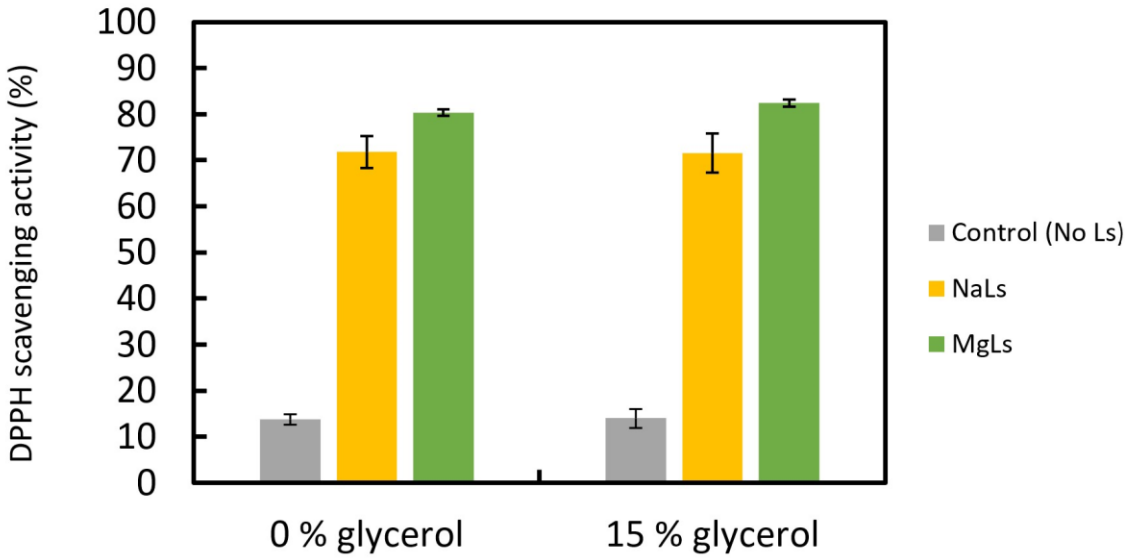

Fig. 7 - Antioxidant activity (DPPH scavenging) of the produced films.

3.6. Assessment of the performance of the films on the preservation of a food matrix

Considering the results obtained in the characterization of the films, and the fact that the goal of this work was to prepare functional wood inspired films for active packaging, it was decided that the films performance on the preservation of a food matrix model should be assessed. For comparison purposes, commercial LDPE films were also used. In this sense, minimally processed and freshly cut pears were packaged, as shown in Fig. 8 (A), and stored at 4.0 ± 1.0 °C for 7 days, in the refrigerator, and evaluated in the 3rd and 7th day of storage regarding their visual appearance, BI, weight loss and pH, parameters that are related to fruit quality and consumers acceptance (Rodríguez et al., 2020). As can be observed in Fig. 8 (B), the visual appearance of the fruits confirmed that the prepared films were able to preserve the packaged fruit samples better than the LPDE commercial film or the fruit stored without any film. This is due to presence of the lignosulfonates in the nanocomposite films that as a result of their antioxidant properties inhibited the polyphenol oxidase activity (Sayavedra-Soto & Montgomery, 1986). The enzymatic browning happens predominantly due to the oxidation of phenolic compounds present in the fruit via polyphenol oxidase, that promotes the formation of o-quinone, which polymerizes producing melanin, a brown pigment (Borges et al., 2016; Sayavedra-Soto & Montgomery, 1986; Shrestha et al., 2020). Similar effects have been observed when fresh cut apples and potatoes were packaged with films with shallot and onion waste extracts, which are also rich sources of polyphenols and antioxidants (Thivya et al., 2021). The visual appearance of the packaged fruits is in accordance with the values of BI of the packaged pears, as depicted in Fig. 9 (A). Freshly cut pears present a BI index of 16.79 ± 0.97 that increased after 7 days at 4.0 ± 1.0 °C for all packed samples. However, it is clear that the films with lignosulfonates delayed the browning of the stored fruits (Be-NaLs-0gly: 24.37 ± 0.80; Be-NaLs-15gly: 22.09 ± 0.96; Be-MgLs-0gly: 20.31 ± 0.68; Be-MgLs-15gly: 19.20 ±

0.62) when compared fruits stored with no film (99.79 ± 0.92) or with LDPE commercial film (37.46 ± 0.87).

Regarding the weight loss of the fruit over the storage time, the results presented in Fig. 9 (B) show a clear trend of increasing weight loss over time. After the 7 days of storage, the freshly cut pears packaged without a film presented the highest weight loss value (36.27 ± 0.58 %), while the fruits packaged with commercial LDPE film presented the lowest one (5.32 ± 0.65 %). The fruits packaged with the prepared nanocomposite films present weight loss values of 10.75 ± 0.23 % and 19.86 ± 0.89 %, for the Be-NaLs-0gly and Be-NaLs-15gly films, respectively, and 8.71 ± 0.86 % and 17.30 ± 0.90 % for the Be-MgLs-0gly and Be-MgLs-15gly, respectively. Similar results were reported for avocados packaged with chitosan and carboxymethyl cellulose (CMC) films containing moringa extracts (Tesfay, 2016) or cherry tomatoes and grapes packaged with chitosan, gelatin and methylcellulose films with tannic acid (Halim et al., 2018).

Changes in the pH values of the fruit are indicative of physiological changes. Therefore, the evaluation of this parameter after storage is of high importance to assess the fruit quality and the consumers acceptance. In Fig. 9 (C), the results of the evolution of pH of the pears over storage time are presented. Initially, the pears present a pH value of 5.34 ± 0.02, but after 7 days of storage, a significant decrease in pH is observed, for the fruits package without a film (5.00 ± 0.03). After 7 days, a similar significant decrease was observed on the storage of the fruits with the commercial LDPE film, where the fruits present a pH value of 5.04 ± 0.02. On the other hand, the fruits packaged with the films containing lignosulfonates present a significant lower decrease of values of pH (Be-NaLs-0gly: 5.17 ± 0.02; Be-NaLs-15gly: 5.25 ± 0.01; Be-MgLs-0gly: 5.22 ± 0.01; Be-MgLs-15gly: 5.28 ± 0.02)) when comparing to the initial values of

pH of the fruit (5.34 ± 0.02), suggesting a better performance of the nanocomposite films in delaying the decrease of the packaged fruits pH.

Overall, the prepared films show a superior performance in delaying the browning of the fruit and delaying the decrease of their pH, which are critical properties to maintain the quality of fruits.

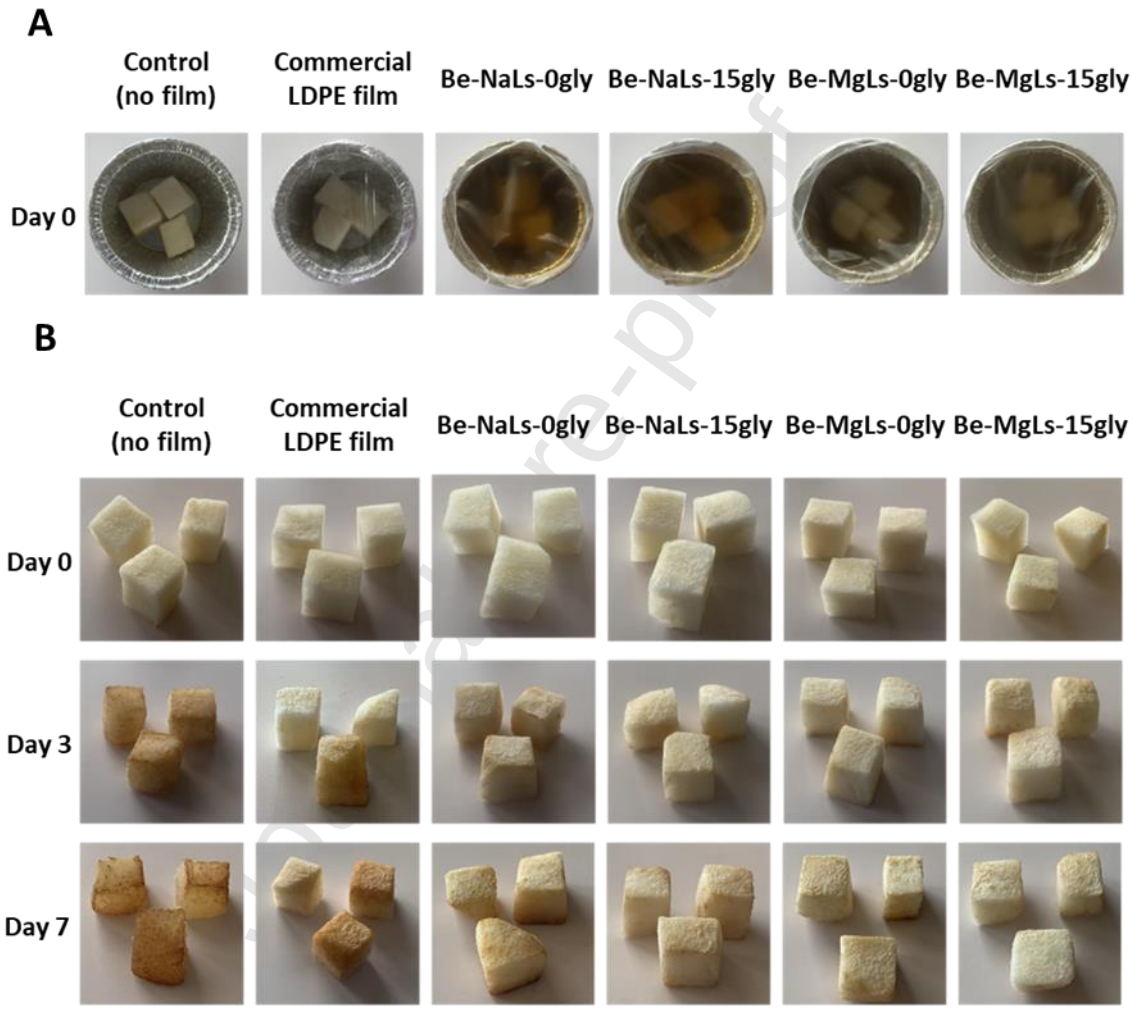

Fig. 8 - (**A**) Digital photos of the packaged fruits with the prepared nanocomposite films and (**B**) Visual appearance of the freshly cut pears before and after 3 and 7 days of storage at 4 ºC, in the refrigerator.

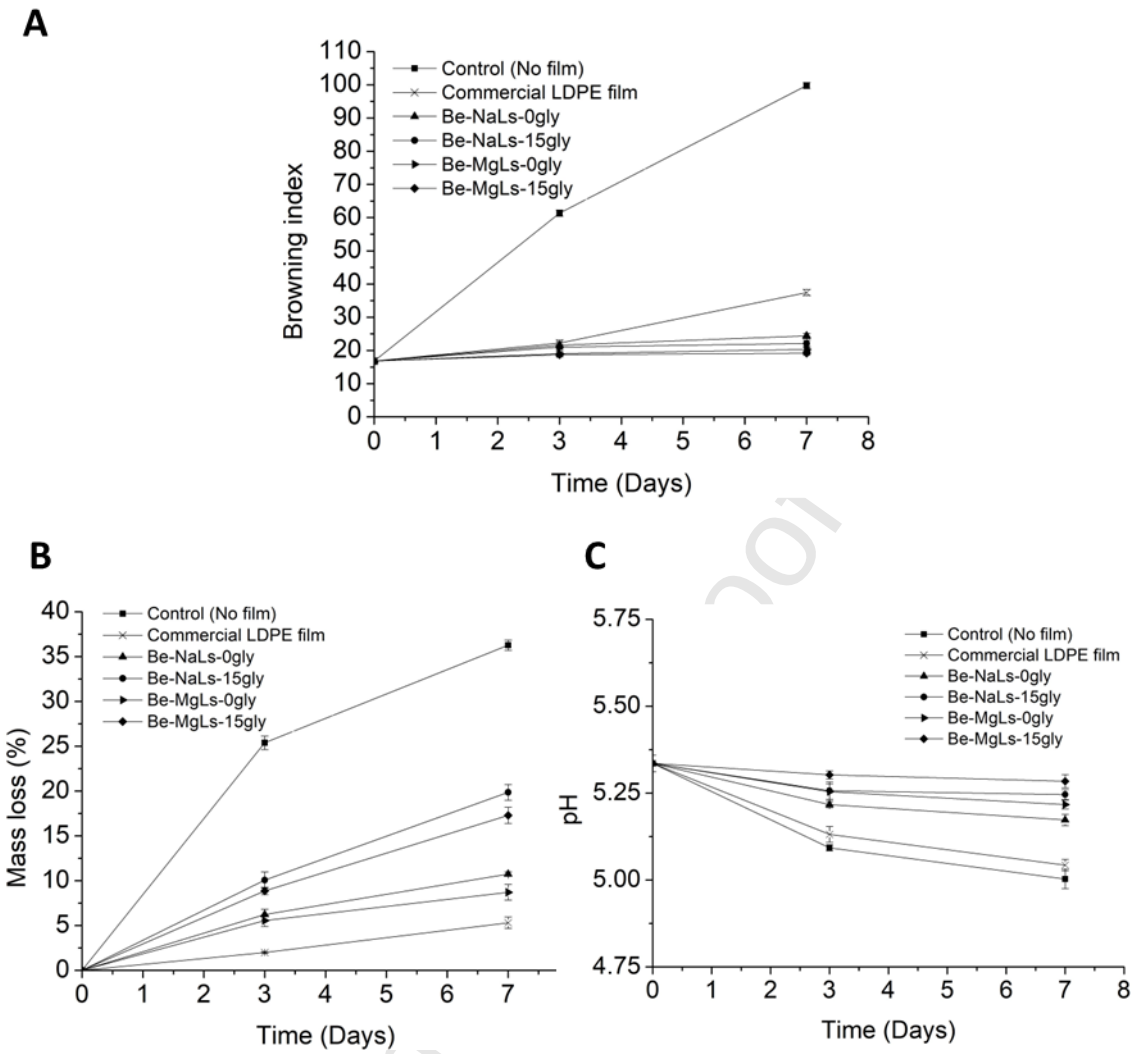

Fig. 9 - (**A**) BI of the fruits at the 3rd and 7th day of storage, (**B**) Weight loss percentage of the fruits at the 3rd and 7th day of storage and (**C**) pH evolution of the freshly cut pears before and after 3 and 7 days of storage at 4 ºC, in the refrigerator.

4. Conclusions

Wood inspired biopolymeric nanocomposite films composed of xylans, cellulose nanofibers and lignosulfonates were successfully produced by solvent casting. All the prepared films showed good homogeneity and thermal stability up to 153 °C, which is a key aspect for food related applications, since these films can withstand typical sterilization procedures. Also, all films displayed good mechanical properties (tensile

strength up to 12.75 – 14.02 MPa), UV-light barrier properties (transmittance ≤ 19.1 % (200 – 400 nm)) and antioxidant activity (up to 82.4% (DPPH scavenging activity). Furthermore, the potential of the nanocomposite films was assessed by testing it in the packaging of freshly cut pears stored at 4 ºC, during 7 days, showing that the produced films have superior performance by delaying the browning and the pH decrease of the fruits, when compared to the commercial LDPE films.

Future studies could include lignosulfonates with other cations that could impart additional functional properties to the developed films.

The combination of the films properties paired with the results of their performance on the preservation of a food matrix shows that the prepared films are relevant sustainable alternatives to the fossil fuel-based packaging currently available on the market.

Credit authorship statement

José M. Silva: Investigation; Writing – original draft, review & editing. Carla Vilela: Writing – review & editing. Ana Violeta Girão: Investigation; Pedro C. Branco: Funding acquisition; Writing – review & editing. João Martins: Funding acquisition; Resources; Writing – review & editing. Mara G. Freire: Writing – review & editing. Armando J. D. Silvestre: Funding acquisition; Resources; Supervision; Writing – review & editing. Carmen S. R. Freire – Conceptualization; Funding acquisition; Project administration; Resources; Supervision; Writing – review & editing.

Funding

This work was developed within the scope of the projects CICECO-Aveiro Institute of Materials (UIDB/50011/2020, UIDP/50011/2020 and LA/P/0006/2020), financed by

national funds through the FCT/MECTES (PIDDAC). FCT is also acknowledged for research contracts under Scientific Employment Stimulus to C.S.R.F. (CEECIND/00464/2017) and C.V. (2021.01571.CEECIND). The authors would also like to acknowledge Celbi – Celulose da Beira Industrial, SA and The Navigator Company for funding the PhD scholarship.

References

Achachlouei, B. F., & Zahedi, Y. (2018). Fabrication and characterization of CMC-based nanocomposites reinforced with sodium montmorillonite and TiO2 nanomaterials. *Carbohydrate Polymers*, *199*(2), 415–425. https://doi.org/10.1016/j.carbpol.2018.07.031

Alexandri, M., Papapostolou, H., Komaitis, M., Stragier, L., Verstraete, W., Danezis, G. P., Georgiou, C. A., Papanikolaou, S., & Koutinas, A. A. (2016). Evaluation of an integrated biorefinery based on fractionation of spent sulphite liquor for the production of an antioxidant-rich extract, lignosulphonates and succinic acid. *Bioresource Technology*, *214*(8), 504–513. https://doi.org/10.1016/j.biortech.2016.03.162

Andrade-Pizarro, R. D., Skurtys, O., & Osorio-Lira, F. (2015). Effect of cellulose nanofibers concentration on mechanical, optical, and barrier properties of gelatin-based edible films. *DYNA*, *82*(191), 219–226. https://doi.org/10.15446/dyna.v82n191.45296

Ansari, I. A., & Datta, A. K. (2003). An overview of sterilization methods for packaging materials used in aseptic packaging systems. *Transactions of the Instituion of Chemical Engineers*, *81*(Part C), 1–5. https://doi.org/10.1205/096030803765208670.

Aro, T., & Fatehi, P. (2017). Production and Application of Lignosulfonates and Sulfonated Lignin. *ChemSusChem*, *10*(9), 1861–1877. https://doi.org/10.1002/cssc.201700082

ASTM International. (2022). *Standart Test Methods for Gravimetric Determination of Water Vapor Transmission Rate of Materials (E96/E96M − 22a)* (Issue 2 E96/E96M − 22a). https://doi.org/DOI: 10.1520/E0096_E0096M-05

Basiak, E., Lenart, A., & Debeaufort, F. (2018). How Glycerol and Water Contents Affect the Structural and Functional Properties of Starch-Based Edible Films. *Polymers*, *10*(4), 1–18. https://doi.org/10.3390/polym10040412

Bastarrachea, L., Dhawan, S., & Sablani, S. S. (2011). Engineering Properties of Polymeric-Based Antimicrobial Films for Food Packaging. *Food Engineering Reviews*, *3*(2), 79–93. https://doi.org/10.1007/s12393-011-9034-8

Battisti, R., Fronza, N., Júnior, Á. V., Silveira, S. M. da, Damas, M. S. P., & Quadri, M. G. N. (2017). Gelatin-coated paper with antimicrobial and antioxidant effect for beef packaging. *Food Packaging and Shelf Life*, *11*, 115–124. https://doi.org/10.1016/j.fpsl.2017.01.009

Berglund, J., Mikkelsen, D., Flanagan, B. M., Dhital, S., Gaunitz, S., Henriksson, G., Lindström, M. E., Yakubov, G. E., Gidley, M. J., & Vilaplana, F. (2020). Wood hemicelluloses exert distinct biomechanical contributions to cellulose fibrillar networks. *Nature Communications*, *11*(1), 1–16. https://doi.org/10.1038/s41467-020-18390-z

Bhatia, K., Asrey, R., Jha, S. K., Singh, S., & Kannaujia, P. K. (2013). Influence of packaging material on quality characteristics of minimally processed Mridula pomegranate (Punica granatum) arils during cold storage. *Indian Journal of Agricultural Sciences*, *83*(8), 872–876.

Borges, C. D., Mendonça, C. R. B., Nogueira, D., Hartwig, E. S., & Rutz, J. K. (2016). Conservation of minimally processed apples using edible coatings made of turnip extract and xanthan gum. *Brazilian Journal of Food Technology*, *19*(2), 1–8. https://doi.org/10.1590/1981-6723.3815

Carvalho, J. P. F., Freire, C. S. R., & Vilela, C. (2021). Chapter 9 - Active Packaging. In C. M. Galanakis (Ed.), *Sustainable Food Processing and Engineering* (First, pp. 315–341). https://doi.org/https://doi.org/10.1016/C2019-0-04596-7

Cerqueira, M. A., Souza, B. W. S., Teixeira, J. A., & Vicente, A. A. (2012). Effect of glycerol and corn oil on physicochemical properties of polysaccharide films - A comparative study. *Food Hydrocolloids*, *27*(1), 175–184. https://doi.org/10.1016/j.foodhyd.2011.07.007

Chollakup, R., Pongburoos, S., Boonsong, W., Khanoonkon, N., Kongsin, K., Sothornvit, R., Sukyai, P., Sukatta, U., & Harnkarnsujarit, N. (2020). Antioxidant and antibacterial activities of cassava starch and whey protein blend films containing rambutan peel extract and cinnamon oil for active packaging. *LWT - Food Science and Technology*, *130*(2), 1–11. https://doi.org/10.1016/j.lwt.2020.109573

Das, P., Borah, P. P., & Badwaik, L. S. (2018). Transformation of Chicken Feather Keratin and Pomelo Peel Pectin into Biodegradable Composite Film. *Journal of Polymers and the Environment*, *26*(5), 2120–2129. https://doi.org/10.1007/s10924-017-1109-z

Eslami, Z., Elkoun, S., Robert, M., & Adjallé, K. (2023). A Review of the Effect of Plasticizers on the Physical and Mechanical Properties of Alginate-Based Films. *Molecules*, *28*(18), 1–33. https://doi.org/10.3390/molecules28186637

Esposito, T., Silva, N. H. C. S., Almeida, A., Silvestre, A. J. D., Piccinelli, A., Aquino,

R. P., Sansone, F., Mencherini, T., Vilela, C., & Freire, C. S. R. (2020). Valorisation of chestnut spiny burs and roasted hazelnut skins extracts as bioactive additives for packaging films. *Industrial Crops and Products*, *151*, 112491. https://doi.org/10.1016/j.indcrop.2020.112491

Fiorentino, G., Ripa, M., & Ulgiati, S. (2017). Chemicals from biomass: technological versus environmental feasibility. A review. *Biofuels, Bioproducts and Biorefining*, *11*(1), 195–214. https://doi.org/10.1002/bbb

Flórez, M., Guerra-Rodríguez, E., Cazón, P., & Vázquez, M. (2022). Chitosan for food packaging: Recent advances in active and intelligent films. *Food Hydrocolloids*, *124*(B), 1–16. https://doi.org/10.1016/j.foodhyd.2021.107328

Foster, E. J., Moon, R. J., Agarwal, U. P., Bortner, M. J., Bras, J., Camarero-Espinosa, S., Chan, K. J., Clift, M. J. D., Cranston, E. D., Eichhorn, S. J., Fox, D. M., Hamad, W. Y., Heux, L., Jean, B., Korey, M., Nieh, W., Ong, K. J., Reid, M. S., Renneckar, S., … Youngblood, J. (2018). Current characterization methods for cellulose nanomaterials. *Chemical Society Reviews*, *47*(8), 2609–2679. https://doi.org/10.1039/c6cs00895j

Fu, G.-Q., Su, L. Y., Yue, P.-P., Huang, Y.-H., Bian, J., Li, M.-F., Peng, F., & Sun, R.-C. (2019). Syntheses of xylan stearate nanoparticles with loading function from by-products of viscose fiber mills. *Cellulose*, *26*(12), 7195–7206. https://doi.org/10.1007/s10570-019-02624-5

Gao, C., Pollet, E., & Averous, L. (2017). Properties of glycerol-plasticized alginate films obtained by thermomechanical mixing. *Food Hydrocolloids, 2*(63), 414–420. https://doi.org/10.1016/j.indcrop.2020.112491.

Ghosh, T., Priyadarshi, R., Krebs de Souza, C., Angioletti, B. L., & Rhim, J.-W. (2022). Advances in pullulan utilization for sustainable applications in food packaging and

preservation: A mini-review. *Trends in Food Science & Technology*, *125*(4), 43–53. https://doi.org/10.1016/j.tifs.2022.05.001

Gonçalves, S. M., Santos, D. C. dos, Motta, J. F. G., Santos, R. R. dos, Chávez, D. W. H., & Melo, N. R. de. (2019). Structure and functional properties of cellulose acetate films incorporated with glycerol. *Carbohydrate Polymers*, *209*(1), 190–197. https://doi.org/10.1016/j.carbpol.2019.01.031

Gong, J., Li, J., Xu, J., Xiang, Z., & Mo, L. (2017). Research on cellulose nanocrystals produced from cellulose sources with various polymorphs. *RSC Advances*, *7*(53), 33486–33493. https://doi.org/10.1039/c7ra06222b

Goodfellow. (2023). *LDPE Film 0.025 mm thick 600mm ET31-FM-000126*. https://www.goodfellow.com/p/et31-fm-000126/ldpe-film

Gopinatha Kurup, G., Adhikari, B., & Zisu, B. (2019). Recovery of proteins and lipids from dairy wastewater using food grade sodium lignosulphonate. *Water Resources and Industry*, *22*(3), 1–11. https://doi.org/10.1016/j.wri.2019.100114

Halim, A. L. A., Kamari, A., & Philip, E. (2018). Chitosan, gelatin and methylcellulose films incorporated with tannic acid for food packaging. *International Journal of Biological Macromolecules*, *120*(9), 1119–1126. https://doi.org/10.1016/j.ijbiomac.2018.08.169

Halloub, A., Raji, M., Essabir, H., Chakchak, H., Boussen, R., Bensalah, M. ouadi, Bouhfid, R., & Qaiss, A. el kacem. (2022). Intelligent food packaging film containing lignin and cellulose nanocrystals for shelf life extension of food. *Carbohydrate Polymers*, *296*(5), 119972. https://doi.org/10.1016/j.carbpol.2022.119972

Jakab, E., Faix, O., Till, F., & Székely, T. (1991). Thermogravimetry/Mass Spectrometry of Various Lignosulfonates as well as of a Kraft and Acetosolv

Lignin. *Holzforschung*, *45*(5), 355–360. https://doi.org/10.1515/hfsg.1991.45.5.355

Júnior, L. M., Rodrigues, P. R., Silva, R. G. da, Vieira, R. P., & Alves, R. M. V. (2021). Sustainable Packaging Films Composed of Sodium Alginate and Hydrolyzed Collagen: Preparation and Characterization. *Food and Bioprocess Technology*, *14*(12), 2336–2346. https://doi.org/10.1007/s11947-021-02727-7

Karimi-Khorrami, N., Radi, M., Amiri, S., Abedi, E., & McClements, D. J. (2022). Fabrication, characterization, and performance of antimicrobial alginate-based films containing thymol-loaded lipid nanoparticles: Comparison of nanoemulsions and nanostructured lipid carriers. *International Journal of Biological Macromolecules*, *207*(3), 801–812. https://doi.org/10.1016/j.ijbiomac.2022.03.149

Katahira, R., & Elder, T. J. (2018). Chapter 1: A Brief Introduction to Lignin Structure. In G. T. Beckham (Ed.), *Lignin Valorization: Emerging Approaches* (First edit, pp. 1–20). Royal Society of Chemistry. https://doi.org/10.1039/9781788010351-00001

Kibar, E. A. A., & Us, F. (2017). Starch–Cellulose Ether Films: Microstructure and Water Resistance. *Journal of Food Process Engineering*, *40*(2), 1–8. https://doi.org/10.1111/jfpe.12382

Lemes, A. P., Soto-Oviedo, M. A., Waldman, W. R., Innocentini-Mei, L. H., & Durán, N. (2010). Effect of Lignosulfonate on the Thermal and Morphological Behavior of Poly(3-hydroxybutyrate-co-3-hydroxyvalerate). *Journal of Polymers and the Environment*, *18*(3), 250–259. https://doi.org/10.1007/s10924-010-0170-7

Leon-Tinoco, A. Y., Annis, S. L., Almeida, S. T., Guimarães, B. C., Killerby, M., Zhang, J., Wu, C., Perkins, L. B., Ma, Z., Jeong, K. C., & Romero, J. J. (2022). Evaluating the potential of lignosulfonates and chitosans as alfalfa hay preservatives using in vitro techniques. *Journal of Animal Science*, *100*(6), 1–15. https://doi.org/10.1093/jas/skac154

Li, H., Xue, Y., Wu, J., Wu, H., Qin, G., Li, C., Ding, J., Liu, J., Gan, L., & Long, M. (2016). Enzymatic hydrolysis of hemicelluloses from Miscanthus to monosaccharides or xylo-oligosaccharides by recombinant hemicellulases. *Industrial Crops and Products*, *79*(11), 170–179. https://doi.org/10.1016/j.indcrop.2015.11.021

Liu, L., Cui, B., Tan, L., & Wang, W. (2021). Improving the combination of cellulose and lignin using xylan as a compatibilizer. *Cellulose*, *28*(9), 5335–5349. https://doi.org/10.1007/s10570-021-03864-0

Liu, Y., Liu, Y., Han, K., Cai, Y., Ma, M., Tong, Q., & Sheng, L. (2019). Effect of nano-TiO2 on the physical, mechanical and optical properties of pullulan film. *Carbohydrate Polymers*, *218*, 95–102. https://doi.org/10.1016/j.carbpol.2019.04.073

Longwei, J., Luo, Z., Liu, H., Wang, F., Li, H., Gao, H., & Zhang, H. (2021). Preparation and Characterization of Chitosan Films Containing Lychee (Litchi chinensis Sonn.) Pericarp Powder and Their Application as Active Food Packaging. *Foods*, *10*(11), 2834. https://doi.org/10.3390/foods10112834

López, O. V., Ninago, M. D., Lencina, M. M. S., García, M. A., Andreucetti, N. A., Ciolino, A. E., & Villar, M. A. (2015). Thermoplastic starch plasticized with alginate-glycerol mixtures: Melt-processing evaluation and film properties. *Carbohydrate Polymers*, *126*(1), 83–90. https://doi.org/10.1016/j.carbpol.2015.03.030

Mena-Cervantes, V. Y., Hernández-Altamirano, R., & Tiscareño-Ferrer, A. (2020). Development of a green one-step neutralization process for valorization of crude glycerol obtained from biodiesel. *Environmental Science and Pollution Research*, *23*(27), 28500–28509. https://doi.org/10.1007/s11356-019-07287-0

Miao, Z., Zhang, Y., & Lu, P. (2021). Novel active starch films incorporating tea polyphenols-loaded porous starch as food packaging materials. *International Journal of Biological Macromolecules*, *192*(10), 1123–1133. https://doi.org/10.1016/j.ijbiomac.2021.09.214

Morais, E. S., Mendonça, P. V., Coelho, J. F. J., Freire, M. G., Freire, C. S. R., Coutinho, J. A. P., & Silvestre, A. J. D. (2018). Deep Eutectic Solvent Aqueous Solutions as Efficient Media for the Solubilization of Hardwood Xylans. *ChemSusChem*, *11*(4), 753–762. https://doi.org/10.1002/cssc.201702007

Moreirinha, C., Vilela, C., Silva, N. H. C. S., Pinto, R. J. B., Almeida, A., Rocha, M. A. M., Coelho, E., Coimbra, M. A., Silvestre, A. J. D., & Freire, C. S. R. (2020). Antioxidant and antimicrobial films based on brewers spent grain arabinoxylans, nanocellulose and feruloylated compounds for active packaging. *Food Hydrocolloids*, *108*(105836), 1–9. https://doi.org/10.1016/J.FOODHYD.2020.105836

Mostafavi, F. S., & Zaeim, D. (2020). Agar-based edible films for food packaging applications - A review. *International Journal of Biological Macromolecules*, *159*, 1165–1176. https://doi.org/10.1016/j.ijbiomac.2020.05.123

Myrvold, B. O. (2008). A new model for the structure of lignosulphonates Part 1. Behaviour in dilute solutions. *Industrial Crops and Products*, *27*(2), 214–219. https://doi.org/10.1016/j.indcrop.2007.07.010

Naidu, D. S., Hlangothi, S. P., & John, M. J. (2018). Bio-based products from xylan: A review. *Carbohydrate Polymers*, *179*, 28–41. https://doi.org/10.1016/j.carbpol.2017.09.064

Neto, C. P., Silvestre, A. J. D., Evtuguin, D. V., Freire, C. S. R., Pinto, P. C. R., Santiago, A. S., Fardim, P., & Holmbom, B. (2004). Bulk and surface composition

of ECF bleached hardwood kraft pulp fibres. *Nordic Pulp and Paper Research Journal*, *19*(4), 513–520. https://doi.org/10.3183/npprj-2004-19-04-p513-520

Núñez-Flores, R., Giménez, B., Fernández-Martín, F., E., L.-C. M., Montero, M. P., & Gómez-Guillén, M. C. (2012). Role of lignosulphonate in properties of fish gelatin films. *Food Hydrocolloids*, *27*(1), 60–71. https://doi.org/10.1016/j.foodhyd.2011.08.015

O'Brien, F. E. M. (1948). The control of humidity by saturated salt solutions. *Journal of Scientific Instruments*, *25*(3), 73–76. https://doi.org/10.1088/0950-7671/25/3/305

Palou, E., López-Malo, A., Barbosa-Cánovas, G. V., Welti-Chanes, J., & Swanson, B. G. (1999). Polyphenoloxidase Activity and Color of Blanched and High Hydrostatic Pressure Treated Banana Puree. *Journal of Food Science*, *64*(1), 42–45. https://doi.org/10.1111/j.1365-2621.1999.tb09857.x

Pastell, H., Virkki, L., Harju, E., Tuomainen, P., & Tenkanen, M. (2009). Presence of 1→3-linked 2-O-β-D-xylopyranosyl-α-L-arabinofuranosyl side chains in cereal arabinoxylans. *Carbohydrate Research*, *344*(18), 2480–2488. https://doi.org/10.1016/j.carres.2009.09.035

Peng, F., Ren, J. L., Xu, F., Bian, J., Peng, P., & Sun, R. C. (2009). Comparative study of hemicelluloses obtained by graded ethanol precipitation from sugarcane bagasse. *Journal of Agricultural and Food Chemistry*, *57*(14), 6305–6317. https://doi.org/10.1021/jf900986b

Peng, P., Peng, F., Bian, J., Xu, F., & Sun, R. (2011). Studies on the starch and hemicelluloses fractionated by graded ethanol precipitation from bamboo phyllostachys bambusoides f. shouzhu Yi. *Journal of Agricultural and Food Chemistry*, *59*(6), 2680–2688. https://doi.org/10.1021/jf1045766

Ramirez, D. O. S., Carletto, R. A., Tonetti, C., Giachet, F. T., Varesano, A., & Vineis,

C. (2017). Wool keratin film plasticized by citric acid for food packaging. *Food Packaging and Shelf Life*, *12*(4), 100–106. https://doi.org/10.1016/j.fpsl.2017.04.004

Riahi, Z., Priyadarshi, R., Rhim, J. W., Lotfali, E., Bagheri, R., & Pircheraghi, G. (2022). Alginate-based multifunctional films incorporated with sulfur quantum dots for active packaging applications. *Colloids and Surfaces B: Biointerfaces*, *215*(4), 112519. https://doi.org/10.1016/j.colsurfb.2022.112519

Rodríguez, G. M., Sibaja, J. C., Espitia, P. J. P., & Otoni, C. G. (2020). Antioxidant active packaging based on papaya edible films incorporated with Moringa oleifera and ascorbic acid for food preservation. *Food Hydrocolloids*, *103*(105630), 1–12. https://doi.org/10.1016/j.foodhyd.2019.105630

Roy, S., & Rhim, J. (2022). Starch/agar-based functional films integrated with enoki mushroom-mediated silver nanoparticles for active packaging applications. *Food Bioscience*, *49*(10), 101867–101876. https://doi.org/10.1016/j.fbio.2022.101867

Roy, S., & Rhim, J. W. (2021). Preparation of pectin/agar-based functional films integrated with zinc sulfide nano petals for active packaging applications. *Colloids and Surfaces B: Biointerfaces*, *207*(111999), 1–8. https://doi.org/10.1016/j.colsurfb.2021.111999

Sayavedra-Soto, L. A., & Montgomery, M. W. (1986). Inhibition of Polyphenoloxidase by Sulfite. *Journal of Food Science*, *51*(6), 1531–1536. https://doi.org/10.1111/j.1365-2621.1986.tb13852.x

Schnell, C. N., Galván, M. V., Peresin, M. S., Inalbon, M. C., Vartiainen, J., Zanuttini, M. A., & Mocchiutti, P. (2017). Films from xylan/chitosan complexes: preparation and characterization. *Cellulose*, *24*(10), 4393–4403. https://doi.org/10.1007/s10570-017-1411-x

Shafizadeh, F., McGinnis, G. D., & Philpot, C. W. (1972). Thermal degradation of xylan and related model compounds. *Carbohydrate Research*, *25*(1), 23–33. https://doi.org/10.1016/S0008-6215(00)82742-1

Shen, D. K., Gu, S., & Bridgwater, A. V. (2010). Study on the pyrolytic behaviour of xylan-based hemicellulose using TG-FTIR and Py-GC-FTIR. *Journal of Analytical and Applied Pyrolysis*, *87*(2), 199–206. https://doi.org/10.1016/j.jaap.2009.12.001

Shen, Q., Zhang, T., & Zhu, M. F. (2008). A comparison of the surface properties of lignin and sulfonated lignins by FTIR spectroscopy and wicking technique. *Colloids and Surfaces A: Physicochemical and Engineering Aspects*, *320*(1–3), 57–60. https://doi.org/10.1016/j.colsurfa.2008.01.012

Shrestha, L., Kulig, B., Moscetti, R., Massantini, R., Pawelzik, E., Hensel, O., & Sturm, B. (2020). Optimisation of Physical and Chemical Treatments to Control Browning Development and Enzymatic Activity on Fresh-cut Apple Slices. *Foods*, *9*(76), 1–21. https://doi.org/10.3390/foods9010076

Silva, N. H. C. S., Figueira, P., Fabre, E., Pinto, R. J. B., Pereira, M. E., Silvestre, A. J. D., Marrucho, I. M., Vilela, C., & Freire, C. S. R. (2020). Dual nanofibrillar-based bio-sorbent films composed of nanocellulose and lysozyme nanofibrils for mercury removal from spring waters. *Carbohydrate Polymers*, *238*, 116210. https://doi.org/10.1016/j.carbpol.2020.116210

Silva, N. H. C. S., Vilela, C., Almeida, A., Marrucho, I. M., & Freire, C. S. R. (2018). Pullulan-based nanocomposite films for functional food packaging: Exploiting lysozyme nanofibers as antibacterial and antioxidant reinforcing additives. *Food Hydrocolloids*, *77*(4), 921–930. https://doi.org/10.1016/J.FOODHYD.2017.11.039

Sousa, S., Ramos, A., Evtuguin, D. V., & Gamelas, J. A. F. (2016). Xylan and xylan derivatives—Their performance in bio-based films and effect of glycerol addition.

Industrial Crops and Products, *94*(12), 682–689. https://doi.org/10.1016/j.indcrop.2016.09.031

Sun, R., Fang, J., & Rowlands, P. (1998). Physicochemical and Thermal Characterization of Wheat Straw Hemicelluloses and Cellulose. *Polymer Journal*, *30*(4), 289–294. https://doi.org/10.1295/polymj.30.289

Tedeschi, G., Guzman-Puyol, S., Ceseracciu, L., Paul, U. C., Picone, P., Di Carlo, M., Athanassiou, A., & Heredia-Guerrero, J. A. (2020). Multifunctional Bioplastics Inspired by Wood Composition: Effect of Hydrolyzed Lignin Addition to Xylan-Cellulose Matrices. *Biomacromolecules*, *21*(2), 910–920. https://doi.org/10.1021/acs.biomac.9b01569

Tesfay, S. Z. (2016). The efficacy of combined application of edible coating and moringa extract in enhancing fruit quality in avocado (Persea americana Mill). *South African Avocado Growers' Association Yearbook*, *39*(1), 51–58. https://doi.org/10.17660/ActaHortic.2021.1306.32

Theenathayalan, R., Thirisha, S. N., & Suganya, R. (2022). Impact of different concrete ingredients on the microstructure of lightweight concrete – A comprehensive review. *Materials Today: Proceedings*, *62*(Part 6), 4392–4396. https://doi.org/10.1016/j.matpr.2022.04.886

Thivya, P., Bhosale, Y. K., Anandakumar, S., Hema, V., & Sinija, V. R. (2021). Development of active packaging film from sodium alginate/carboxymethyl cellulose containing shallot waste extracts for anti-browning of fresh-cut produce. *International Journal of Biological Macromolecules*, *188*(5), 790–799. https://doi.org/10.1016/j.ijbiomac.2021.08.039

United Nations. (2015). Transforming our world: the 2030 Agenda for Sustainable Development. In *Transforming our world: the 2030 Agenda for Sustainable*

Development. https://doi.org/10.1201/b20466-7

Vianna, T. C., Marinho, C. O., Marangoni Júnior, L., Ibrahim, S. A., & Vieira, R. P. (2021). Essential oils as additives in active starch-based food packaging films: A review. *International Journal of Biological Macromolecules*, *182*(7), 1803–1819. https://doi.org/10.1016/j.ijbiomac.2021.05.170

Vilela, C., Kurek, M., Hayouka, Z., Röcker, B., Yildirim, S., Antunes, M. D. C., Nilsen-Nygaard, J., Pettersen, M. K., & Freire, C. S. R. (2018). A concise guide to active agents for active food packaging. *Trends in Food Science and Technology*, *80*(10), 212–222. https://doi.org/10.1016/j.tifs.2018.08.006

Vilela, C., Morais, J. D., Silva, A. C. Q., Muñoz-Gil, D., Figueiredo, F. M. L., Silvestre, A. J. D., & Freire, C. S. R. (2020). Flexible nanocellulose/lignosulfonates ion-conducting separators for polymer electrolyte fuel cells. *Nanomaterials*, *10*(9), 1–13. https://doi.org/10.3390/nano10091713

Vilela, C., Pinto, R. J. B., Coelho, J., Domingues, M. R. M., Daina, S., Sadocco, P., Santos, S. A. O., & Freire, C. S. R. (2017). Bioactive chitosan/ellagic acid films with UV-light protection for active food packaging. *Food Hydrocolloids*, *73*, 120–128. https://doi.org/10.1016/j.foodhyd.2017.06.037

Xiao, L., Kang, S., Lapu, M., Jiang, P., Wang, X., Liu, D., Li, J., & Liu, M. (2022). Preparation and characterization of chitosan/pullulan film loading carvacrol for targeted antibacterial packaging of chilled meat. *International Journal of Biological Macromolecules*, *211*(6), 140–149. https://doi.org/10.1016/j.ijbiomac.2022.05.044

Yang, H., Yan, R., Chen, H., Lee, D. H., & Zheng, C. (2007). Characteristics of hemicellulose, cellulose and lignin pyrolysis. *Fuel*, *86*(12–13), 1781–1788. https://doi.org/10.1016/j.fuel.2006.12.013

Yildirim, S., Röcker, B., Pettersen, M. K., Nilsen-Nygaard, J., Ayhan, Z., Rutkaite, R., Radusin, T., Suminska, P., Marcos, B., & Coma, V. (2018). Active Packaging Applications for Food. *Comprehensive Reviews in Food Science and Food Safety*, *17*(1), 165–199. https://doi.org/10.1111/1541-4337.12322

Yousefi, P., Hamedi, S., Garmaroody, E. R., & Koosha, M. (2020). Antibacterial nanobiocomposite based on halloysite nanotubes and extracted xylan from bagasse pith. *International Journal of Biological Macromolecules*, *160*(10), 276–287. https://doi.org/10.1016/j.ijbiomac.2020.05.209

Zhang, R., Zhai, X., Wang, W., & Hou, H. (2022). Preparation and evaluation of agar/maltodextrin-beeswax emulsion films with various hydrophilic-lipophilic balance emulsifiers. *Food Chemistry*, *384*(132541), 1–9. https://doi.org/10.1016/j.foodchem.2022.132541

Zhao, W., Liang, X., Wang, X., Wang, S., Wang, L., & Jiang, Y. (2022). Chitosan based film reinforced with EGCG loaded melanin-like nanocomposite (EGCG@MNPs) for active food packaging. *Carbohydrate Polymers*, *290*(119471), 1–11. https://doi.org/10.1016/j.carbpol.2022.119471

Declaration of interests

The authors proclaim that they have no known competing financial interests or personal relationships that could have appeared to influence the work reported in this manuscript.

2nd of November 2023
Carmen Freire